New Phytologist

Research

Kinetic factors of physiology and the dynamic light environment influence the economic landscape of short-term hydraulic risk

Thomas N. Buckley, Ethan H. Frehner and Brian N. Bailey

Department of Plant Sciences, University of California, Davis, Davis, CA 95616, USA

Author for correspondence:
Tom Buckley
Email: tnbuckley@ucdavis.edu

Received: *29 July 2022*
Accepted: *10 January 2023*

New Phytologist (2023)
doi: 10.1111/nph.18739

Key words: optimality, plant hydraulics, stomata, sunflecks, transpiration.

Summary

- Optimality-based models of stomatal conductance unify biophysical and evolutionary constraints and can improve predictions of land-atmosphere carbon and water exchange. Recent models incorporate hydraulic constraints by penalizing excessive stomatal opening in relation to hydraulic damage caused by low water potentials. We used simulation models to test whether penalties based solely on vulnerability curves adequately represent the optimality hypothesis, given that they exclude the effects of kinetic factors on stomatal behavior and integrated carbon balance.
- To quantify the effects of nonsteady-state phenomena on the landscape of short-term hydraulic risk, we simulated diurnal dynamics of leaf physiology for 10 000 patches of leaf in a canopy and used a ray-tracing model, Helios, to simulate realistic variation in sunfleck dynamics.
- Our simulations demonstrated that kinetic parameters of leaf physiology and sunfleck properties influence the economic landscape of short-term hydraulic risk, as characterized by the effect of stomatal strategy (gauged by the water potential causing a 50% hydraulic penalty) on both aggregated carbon gain and the aggregated carbon cost of short-term hydraulic risk.
- Hydraulic penalties in optimization models should be generalized to allow their parameters to account for kinetic factors, in addition to parameters of hydraulic vulnerability.

Introduction

Stomata regulate CO_2 and water vapor exchange between most land plants and the atmosphere. Stomatal behavior influences forest and crop productivity, hydrology, and climate (e.g. Fischer *et al.*, 1998; Reichstein *et al.*, 2002; Bonan, 2008; Choat *et al.*, 2012; Anderegg *et al.*, 2016). Biologists have therefore long sought models for stomatal conductance (g_{sw}; symbols are listed in Table 1) that are reliable and can be parameterized and improved based on physiological knowledge (Farquhar & Wong, 1984; Ball *et al.*, 1987; Damour *et al.*, 2010; Buckley, 2017), and optimization theory is a promising tool to this end (Givnish & Vermeij, 1976; Cowan & Farquhar, 1977; Medlyn *et al.*, 2011; Prentice *et al.*, 2014; Buckley *et al.*, 2017; Lavergne *et al.*, 2020; Wang *et al.*, 2020). Optimization-based models predict stomatal responses from the hypothesis that they maximize carbon gain relative to water loss. Such models diverge in how they quantify the cost of water (Buckley *et al.*, 2017; Wang *et al.*, 2020). Cowan & Farquhar (1977; CF) used a constrained-optimization approach, treating total transpiration over a day as an external constraint. However, the CF solution involves a Lagrange multiplier whose value is not specified by the theory, making it difficult to apply the result, and the approach is agnostic to the risks and costs associated with hydraulic decline. Moreover, since the method of Lagrange multipliers assumes the constraint is invariant with respect to the control parameter, CF tacitly assumes that hydraulics limit daily transpiration independently of variation in stomatal conductance itself. Yet that is inconsistent with the fact that, in most cases, a small increase in g_{sw} at one moment in the day would increase total transpiration without violating hydraulic constraints.

An alternative approach pioneered by Jones & Sutherland (1991), and more recently elaborated and advanced by Wolf *et al.* (2016), Sperry *et al.* (2016, 2017), Eller *et al.* (2018, 2020), and Wang *et al.* (2020) (the 'HP' approach, for hydraulic penalty), instead penalizes high transpiration rates based on their impact on the plant's water transport system. The goal function in HP models is

$$\text{goal function} = A(\psi_{leaf}) - \Theta(\psi_{leaf}), \qquad \text{Eqn 1}$$

where A is net CO_2 assimilation rate, ψ_{leaf} is leaf water potential (≤ 0), and Θ is a *hydraulic penalty function* that differs between models (Table 2 lists the form of Θ in each model). The function Θ increases as ψ_{leaf} declines (and thus as stomatal conductance and transpiration rate increase). In the Sperry, Eller, and Wang models, Θ is explicitly based on the hydraulic vulnerability curve (the decline of plant hydraulic conductance, K_{plant}, as ψ_{leaf} declines; Fig. 1a). For example, in the Eller model, $\Theta = A \cdot (1 - K_{plant}/K_{plant,max}) = A \cdot PLC$, where $K_{plant,max}$ is the value of K_{plant} at a

New Phytologist

Table 1 List of symbols.

Description	Symbol	Units	Default value
CO_2 assimilation rate (mean over time and leaves)	A (**A**)	μmol m^{-2} s^{-1}	–
Rate constant for adjustment of K_{leaf} and K_{stem}	α_K	s^{-1}	0.2
Rate constant for adjustment of $\delta\pi$	α_π	s^{-1}	0.0052/0.0026*
Rate constant for induction of V_{m25}	α_V	s^{-1}	0.0075/0.0045*
Ambient CO_2 mole fraction	c_a	μmol mol^{-1}	400
Aggregated carbon cost of short-term hydraulic risk	C_{risk}	μmol m^{-2} s^{-1}	–
Proportionality factor relating g_{sw} to P_g and P_e	χ	mol m^{-2} s^{-1} MPa^{-1}	0.062
Guard cell osmotic gradient (target)	$\delta\pi$ ($\delta\pi'$)	MPa	–
Leaf-to-air water vapor mole fraction difference	Δw	mol mol^{-1}	–
Leaf transpiration rate	E	mol m^{-2} s^{-1}	–
Stem elastance	e_{stem}	MPa	10.0
Leaf thermal infrared sky-view factor	f_{ir}	–	–
Leaf boundary layer conductance to heat (water vapor)	g_{bh} (g_{bw})	mol m^{-2} s^{-1}	2.67
Minimum value of stomatal conductance	g_{min}	mol m^{-2} s^{-1}	0.005
Stomatal conductance to water vapor (target)	g_{sw} (g_{sw}')	mol m^{-2} s^{-1}	–
Leaf hydraulic conductance (at 25°C) (at $\psi_{leaf} = 0$)	$K_{leaf(25)(max)}$	mol m^{-2} s^{-1} MPa^{-1}	0.006†,‡
Leaf heat capacity	κ_{leaf}	J m^{-2} K^{-1}	–
PPFD at which V_{m25} is induced by half	K_{mv}	μmol m^{-2} s^{-1}	97
Plant hydraulic conductance $(K_{leaf}{}^{-1} + K_{stem}{}^{-1})^{-1}$	K_{plant}	mol m^{-2} s^{-1} MPa^{-1}	–
Stem hydraulic conductance (at 25°C) (at $\psi_{stem} = 0$)	$K_{stem(25)(max)}$	mol m^{-2} s^{-1} MPa^{-1}	0.006†,‡
Leaf mass per unit area	LMA	g m^{-2}	140
Epidermal mechanical advantage	m	–	2
Leaf water content (at saturation)	$n_{leaf(,max)}$	mol $m^{-2}{}_{leaf}$	12‡
Stem water content (at saturation)	$n_{stem(,max)}$	mol $m^{-2}{}_{leaf}$	25‡
Epidermal turgor pressure	P_e	MPa	–
Guard cell turgor pressure	P_g	MPa	–
Percentage loss of hydraulic conductivity (as a fraction)	PLC	–	–
Leaf photosynthetic photon flux density	PPFD	μmol m^{-2} s^{-1}	–
Leaf osmotic pressure at full turgor	π_o	MPa	1.9
Leaf-absorbed shortwave radiation flux	Q_{SW}	J m^{-2} s^{-1}	–
Risk penalty	r	–	–
Leaf relative water content (at turgor loss)	$R_{(tlp)}$	–	0.925§
Air temperature (in kelvins) (max) (min)	$T_{air(K)(max)(min)}$	°C (K)	min: 15, max: 25
Leaf temperature (in kelvins)	$T_{leaf(K)}$	°C (K)	–
Time of day at which $T_{air} = T_{airmax}$	$t_{Tairmax}$	hour of day	13
Maximum carboxylation velocity at 25°C (target value)	V_{m25} (V'_{m25})	μmol m^{-2} s^{-1}	–
Ambient water vapor mole fraction	w_{air}	mol mol^{-1}	0.01
Steepness parameter in risk penalty and vulnerability curves	ξ	–	5.3
Leaf water potential	ψ_{leaf}	MPa	–
Soil water potential	ψ_{soil}	MPa	0
Stem water potential	ψ_{stem}	MPa	–
ψ_{leaf} causing 50% loss of K_{leaf}	ψ_{50leaf}	MPa	−2.0
ψ_{leaf} causing 50% loss of K_{plant}	$\psi_{50plant}$	MPa	−2.0
Water potential at which risk penalty is 0.5	ψ_{50risk}	MPa	–
ψ_{stem} causing 50% loss of K_{stem}	ψ_{50stem}	MPa	−3.3

*$\delta\pi$ or V_{m25} increasing/decreasing; values at †25 °C; ‡zero water potential; §turgor loss. Symbols and values for physical constants are given in the text.

Table 2 Penalty functions used in hydraulic penalty (HP)-type stomatal optimization models.

Model	Penalty function $\Theta(\psi_{leaf})$	Notes
Wolf *et al*. (2016)	Arbitrary function, except that $d\Theta/\delta\psi_{leaf} < 0$ and $d^2\Theta/d{\psi_{leaf}}^2 > 0$	Θ is 'the carbon costs of hydraulic damage'
Sperry *et al*. (2017)	$\Theta = A_{max} \cdot \left(1 - \frac{K(\psi_{leaf}) - K(\psi_c)}{K(\psi_{soil}) - K(\psi_c)}\right)$*	$A_{max} \equiv \max\{A(\psi_{leaf}) \mid \psi_{leaf} \in [\psi_{soil}, \psi_c]\}$
Eller *et al*. (2018)	$\Theta = A \cdot \left(1 - \frac{K(\psi_{leaf})}{K(0)}\right)$	Equivalent to $\Theta = A \cdot \mathrm{PLC}(\psi_{leaf})$
Wang *et al*. (2020)	$\Theta = A \cdot \frac{E(\psi_{leaf})}{E(\psi_c)}$	

ψ_c is the value of ψ_{leaf} that maximizes steady-state transpiration rate, E (Fig. 1a); PLC is the percentage of lost hydraulic conductivity at a given water potential (expressed as a fraction).
*Note that K in the Sperry model is calculated as the integral of conductivity over the whole-plant pressure gradient.

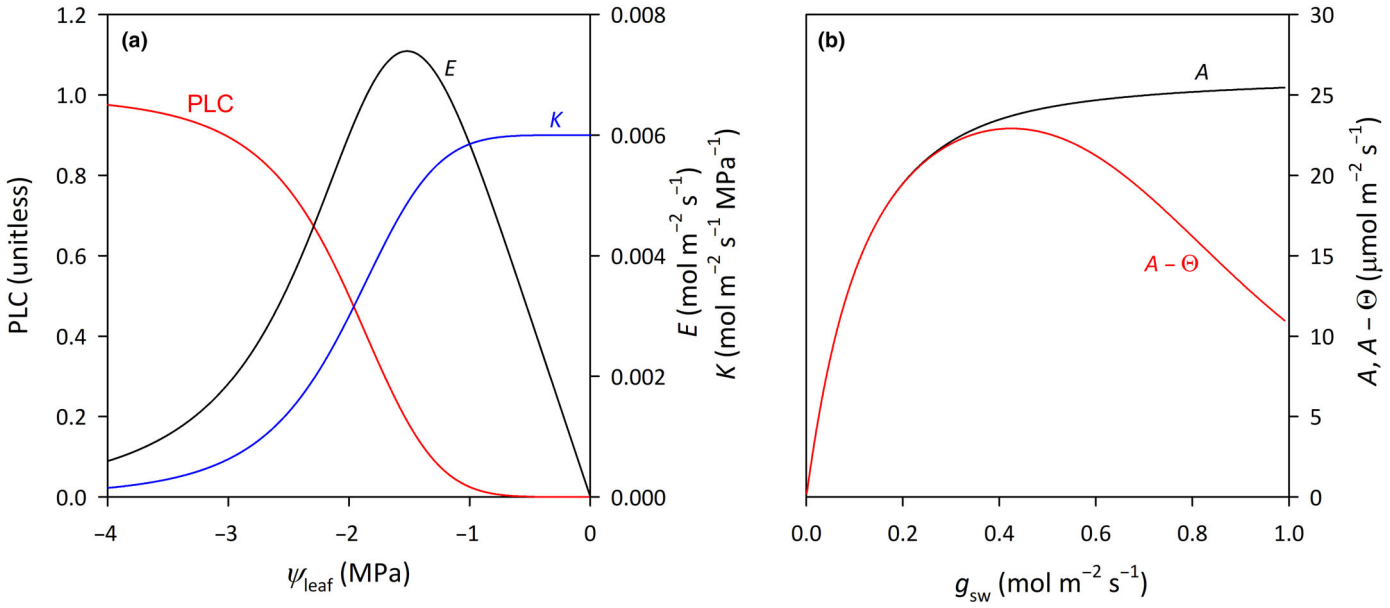

Fig. 1 (a) Sample relationships between leaf water potential (ψ_{leaf}) and hydraulic conductance (K), proportion of lost hydraulic conductivity (PLC), and transpiration rate (E), based on expressions used in the Eller model. (b) Relationship between stomatal conductance (g_{sw}) and the goal function in the Eller model (net CO_2 assimilation rate, A, minus a penalty function Θ, which in the Eller model is equal to the product of A and PLC; un-penalized assimilation rate is shown for reference). PLC, K, E, A, and Θ were calculated using parameter values as follows, and using default values given in Table 1 for all other parameters: water potential causing 50% loss of hydraulic conductance (ψ_{50}) = −2.0 MPa; curvature parameter in vulnerability curve (ξ) = 5.3; hydraulic conductance at zero leaf water potential = 0.006 mol m^{-2} s^{-1} MPa^{-1}; soil water potential = 0; PPFD = 500 μmol m^{-2} s^{-1}; leaf-to-air water vapor mole fraction difference = 0.015 mol mol^{-1}; leaf temperature = 25.0°C.

water potential of zero, and PLC is the percentage of lost hydraulic conductivity, expressed as a fraction (between zero and unity; Fig. 1b).

The HP approach overcomes some of CF's limitations and represents a promising step forward. However, we suggest that the form of the penalty function (Θ) deserves further consideration. The rationale behind penalizing negative water potentials is that they can reduce fitness in ways that are not captured by the current, instantaneous value of photosynthetic rate. These detrimental impacts result chiefly from loss of hydraulic conductivity at low water potentials (effects of water potential on photosynthetic capacity (so-called 'nonstomatal effects'; (e.g. Salvi *et al.*, 2021)) manifest directly in current photosynthesis rate). Hydraulic decline slows water transport, and hence reduces the transpiration rate, stomatal conductance, and photosynthesis rate that can be sustained for a given leaf water potential. If hydraulic decline is severe, as in the case of catastrophic xylem failure, it may kill the leaf or plant (Anderegg *et al.*, 2015; Choat *et al.*, 2018). The resulting costs could be conceived either as an opportunity cost (a decline in future canopy carbon gain) or as a maintenance cost (the carbon cost of sustaining carbon gain by replacing or repairing damaged tissues). The hydraulic penalty, Θ, in HP models is intended to be a proxy for these future costs. For example, Wang *et al.* (2020) referred to Θ as '*a 'shadow cost' or 'risk' to future plant performance*'. Eqn 1, together with any given formulation for the penalty function Θ, defines a *strategy* for current stomatal behavior based on both current and future reductions in carbon gain. Interpreting Eqn 1 as an 'optimization model' is tantamount to claiming that this strategy maximizes fitness, as gauged by the proxy of carbon gain – aggregated to the scale of an individual plant and integrated over its lifetime, and thus incorporating the realized carbon costs of hydraulic risk that are represented instantaneously by the shadow cost Θ.

What determines the risk that future carbon gain will be reduced by hydraulic decline or failure? Clearly, that risk must depend, in part, on the quantities used to calculate Θ in existing HP models – for example, the current degree of hydraulic decline (as in the Eller model) or the proximity of the current transpiration rate to the value that would result in catastrophic xylem failure (as in the Wang model). However, hydraulic risk must also depend on factors that are not included in existing formulations of Θ. For example, the likelihood that catastrophic xylem failure will occur in the near future, given the current value of water potential, depends on the probability that an environmental perturbation will occur that is sufficiently severe to drive steady-state leaf water potential below the threshold for catastrophic failure. The environmental parameter that varies most rapidly and dramatically in plants is usually light intensity (photosynthetic photon flux density or PPFD). An increase in PPFD – for example, when a leaf enters a sunfleck – will warm the leaf, increasing evaporative demand and transpiration rate and thereby reducing water potential. Hydraulic risk should thus depend on the character of such diurnal fluctuations in PPFD. Imagine, for example, two leaves that experience similar average PPFD, but in one case, PPFD is constant over the day, while in the other leaf, PPFD fluctuates dramatically between full sun and full shade. The leaf in the more dynamic environment will likely have a greater probability of xylem failure at any given current value of water

potential than the leaf in the less dynamic environment. Current formulations of Θ do not account for these stochastic and dynamical features of the environment. Moreover, the risk of catastrophic xylem failure should also depend on the probability that leaf water potential could *transiently* exceed the failure threshold. That probability must, in turn, be influenced by kinetic factors that influence the transient dynamics of water potential after environmental perturbations, such as how fast stomata can respond, and the buffering effects of thermal and hydraulic capacitance (heat and water storage) on temperature and water potential. One might hypothesize, for example, that a leaf with very fast-responding stomata should be able to more closely approach the threshold for catastrophic xylem failure than a leaf with very slow-responding stomata, because the faster leaf could 'pull back' from the threshold more rapidly through stomatal closure in the event of sudden water potential decline induced by a rapid environmental change such as a sunfleck. The rate of photosynthetic induction following a change in PPFD may also affect the risk–reward trade-off. Yet, none of these kinetic factors are included in current formulations of Θ.

Our objective in this study was to examine how short-term hydraulic risk (i.e. at a diurnal time scale) is affected by kinetic features of leaf physiology and the dynamic light environment, which together determine transient dynamics of water potential. To capture the dynamic environmental drivers of short-term hydraulic risk, we simulated diurnal dynamics of PPFD for 25 000 leaves (each 5 × 5 cm in size, with PPFD resolved for each 1 × 1 cm patch of leaf) in a canopy using a ray-tracing model, Helios (Bailey, 2018, 2019), and then simulated dynamics of physiology for each of 10 000 randomly selected leaf patches. We sought to ask, more specifically, whether the economic landscape of hydraulic risk – that is, the effect of stomatal behavior on aggregated carbon gain and the aggregated carbon cost of hydraulic risk – is influenced by stochastic and kinetic factors as described previously. In our simulations, we calculated stomatal conductance using the HP model of Eller *et al.* (2020), but modulated stomatal strategy within the general framework of that model by adjusting the water potential at which the penalty function (Θ) equals 50% of net photosynthesis. We calculated the carbon cost of hydraulic risk by comparing aggregated carbon gain between the simulations described above and paired simulations in which hydraulic risk was excluded by setting the ψ_{50} for hydraulic vulnerability to −100 MPa.

Description

Our objective was to determine whether kinetic factors influence the economic landscape of short-term hydraulic risk. By *economic landscape*, we mean the relationship between stomatal 'strategy' (how risky or risk-averse stomatal behavior is) and whole-canopy carbon balance integrated over a day. To quantify that landscape, we needed to allow stomatal strategy to vary widely. We achieved this by predicting stomatal conductance in our simulations (to be described in detail later) using the general HP model framework (Eqn 1), but using a penalty function (Θ) that is defined not by parameters of the hydraulic vulnerability curve, but instead by a tunable parameter, ψ_{50risk}. ψ_{50risk} has no explicit physiological meaning; it is just a tool that we used to represent a range of stomatal strategies. By adjusting the numerical value of ψ_{50risk}, we could simulate a continuum of strategies, from risk-averse (ψ_{50risk} closer to zero) to risky (ψ_{50risk} far below zero). We used the following penalty function:

$$\Theta(\text{this study}) = A \cdot \frac{|\psi_{leaf}|^{\xi}}{|\psi_{50risk}|^{\xi} + |\psi_{leaf}|^{\xi}} \quad \text{Eqn 2}$$

Eqn 2 has the same mathematical form as the penalty function used by Eller *et al.* (2018, 2020), except that one parameter in the Eller version (namely ψ_{50}, the water potential causing 50% loss of hydraulic conductivity) has been replaced with a new, and totally unrelated, parameter: the tunable parameter ψ_{50risk}. (Our model still *depends* on the hydraulic ψ_{50} – it influences how hydraulic conductance declines in relation to water potential – but the numerical value of ψ_{50} was the same across simulations.)

To quantify the economic landscape of short-term hydraulic risk, we simulated diurnal trends in gas exchange for 10 000 patches of leaf within a canopy. We repeated these simulations for a range of stomatal strategies, each represented by a different numerical value of the tunable parameter ψ_{50risk}. For each strategy (each value of ψ_{50risk}), we calculated the average whole-day rate of carbon gain among the 10 000 leaf patches (symbolized **A**, in bold and Roman type to distinguish it from the instantaneous and leaf-scale net CO_2 assimilation rate, A). We also quantified the carbon cost of hydraulic risk, C_{risk}, by repeating all simulations while excluding hydraulic risk by pretending that hydraulic conductance was not affected by changes in water potential. Thus, for each stomatal strategy, we computed two values of **A**: one from simulations with hydraulic risk, and one without. We calculated C_{risk} as the difference between these two values of **A**.

The economic landscape of hydraulic risk is thus represented by two relationships: one between ψ_{50risk} and **A**, and one between ψ_{50risk} and C_{risk}. To determine whether that landscape was affected by kinetic parameters, such as the rate constants for stomatal responses to the environment (α_{π}) or photosynthetic induction in fluctuating light (α_V), or the leaf water content at saturation (SWC), we repeated all of the simulations described above many times – each time adjusting one kinetic parameter in isolation, and generating new relationships between ψ_{50risk} and **A** and C_{risk}. This allowed us to see whether, for example, the economic landscape differed between plants with slow vs fast stomata (low vs high α_{π}).

We also asked three ancillary questions: to what extent do the effects of kinetics on hydraulic risk depend on (1) whether leaf hydraulic decline can be rapidly reversed, (2) sunfleck dynamics, and (3) soil drought? By default, the model assumed K_{leaf} decline was irreversible within a single day; to address (1), we repeated all simulations assuming K_{leaf} decline was immediately reversible. To address (2) and (3), we repeated simulations for canopies differing in structure and leaf angle distribution (LAD; which

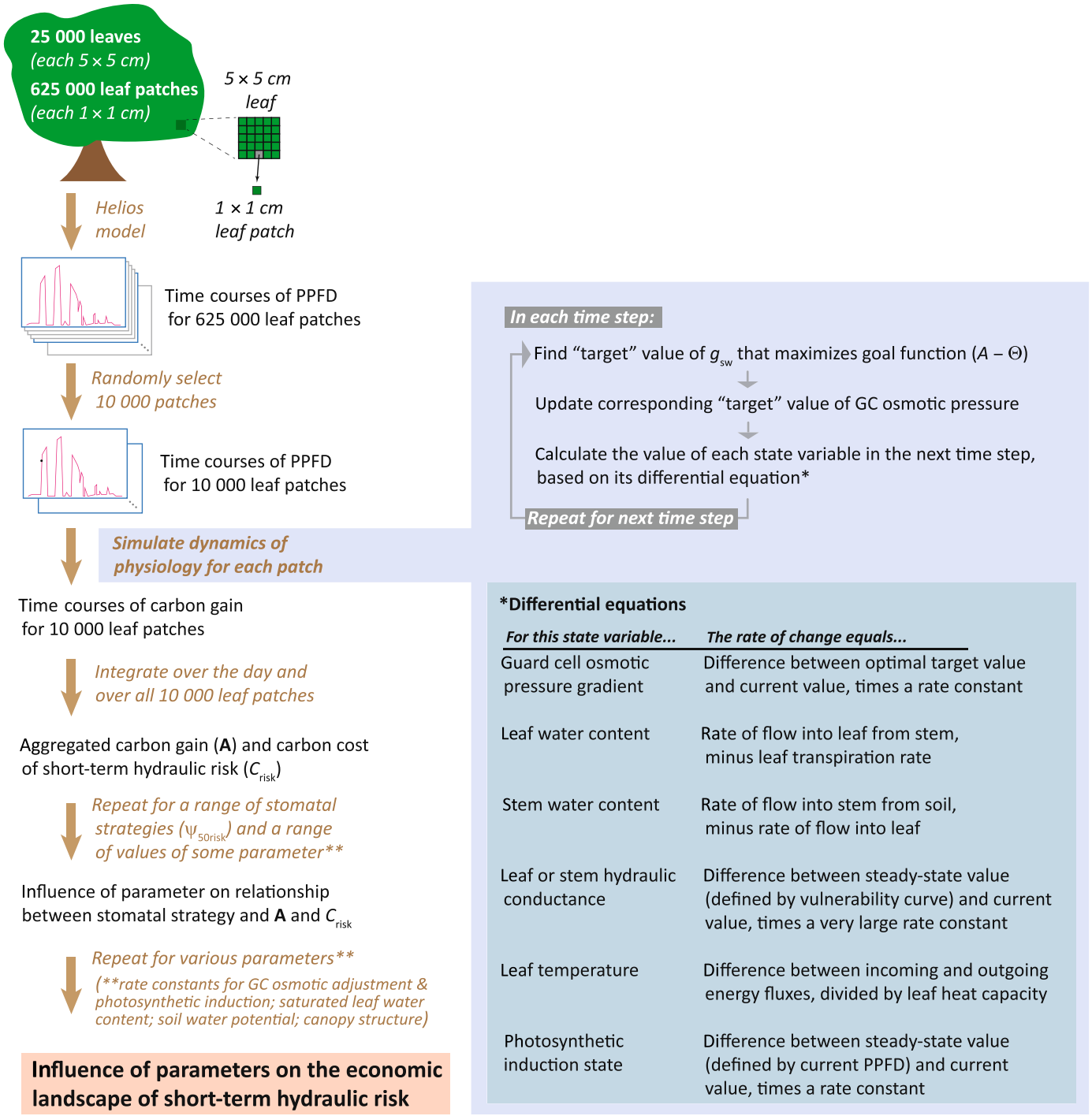

Fig. 2 Diagram illustrating the logical flow of simulations performed in this study. Mathematical expressions for differential equations are given in Appendix A1. Not shown here are additional simulations performed on a subset of 500 leaf patches for parameter sensitivity analysis, and calculations performed to quantify the strength of sunflecks in PPFD time courses. Symbols: g_{sw}, stomatal conductance; A, leaf net CO_2 assimilation rate; Θ, penalty function for optimal stomatal conductance; GC, guard cell; **A**, mean value of A over the day and all leaves in the canopy; C_{risk}, difference in **A** between simulations with and without hydraulic risk.

influence sunfleck properties), and for different values of soil water potential, respectively; for (2) and (3), we used a subset of 500 leaf patches instead of all 10 000.

Fig. 2 illustrates the general logical flow of these simulations and the underlying calculations, and Table 3 provides a list of simulations.

Summary of dynamic model

This section briefly summarizes how we simulated dynamics of PPFD and leaf physiological variables over 1 d for each of many leaf patches in a canopy; additional details are given in Appendix A1.

Table 3 List of simulations.

Description	Figure(s)
I. Simulations at 20 values of ψ_{50risk} × with/ without hydraulic risk	
I(a). standard simulations	
All parameters set at default values given in Table 1	Figs 3–8, 10, S6(a)
I(b). varying kinetic parameters	
Slow vs fast stomata (α_π = 50% smaller or larger)	Fig. 5
slow vs fast photosynthetic induction (α_V = 50% smaller or larger)	Fig. S4
Low vs high leaf water content ($n_{leaf,max}$ = 50% smaller or larger)	Fig. 6
I(c). varying crown structure and LAD	
Spherical crowns + spherical LAD	Fig. S6(b)
Spherical crowns + planophile LAD	Fig. S6(c)
Spherical crowns + erectophile LAD	Fig. S6(d)
II(c). varying soil water potential (ψ_{soil}) (subset of 500 leaf patches)	
Varying ψ_{soil} between −1.8 and 0 MPa	Fig. 9
II. Parameter sensitivity analyses (ψ_{50risk} = −2.0 MPa)	
II(a). varying parameters from 75 to 125% of default values	
Plant parameters	Figs S9–S11
Environmental parameters	Fig. S12
II(b). varying epidermal mechanical advantage (m)	
Varying *m* between 0 and 4	Fig. S13

Except where noted, simulations used Helios output for 10 000 leaf patches from a uniform, laterally continuous crown with spherical leaf angle distribution (LAD), and default values for all parameters given in Table 1.

PPFD dynamics We computed diurnal PPFD dynamics at 0.1 Hz for 25 000 leaves (each 5 × 5 cm square) in a canopy, using a reverse ray-tracing model, Helios (Bailey, 2019), with PPFD resolved for each 1 × 1 cm patch in each leaf (25 patches per leaf). We randomly selected 10 000 leaf patches and simulated diurnal dynamics of physiology for each of those patches.

Gas exchange At each point in time, we identified a *target value* for stomatal conductance (g_{sw}) by maximizing the goal function in Eqn 1 with respect to g_{sw}, using the penalty function given by Eqn 2. The leaf dynamically seeks this target value for g_{sw} by adjusting the osmotic pressure of its stomatal guard cells (Haefner *et al.*, 1997). We calculated stomatal conductance from guard cell osmotic pressure using a hydromechanical model that includes the effects of dynamically varying leaf water potential on guard and epidermal cell turgor pressures (Sharpe *et al.*, 1987; Haefner *et al.*, 1997; Buckley *et al.*, 2003), which allows the model to capture transient features of stomatal behavior, such as the 'wrong-way response' (Buckley & Mott, 2002; Buckley *et al.*, 2011). The goal function requires a value for assimilation rate (A), which we calculated from the biochemical model of Farquhar *et al.* (1980); Supporting Information Methods S1, based on instantaneous values of stomatal conductance, leaf temperature, and photosynthetic capacity.

Dynamics of water content, temperature, and photosynthetic induction state In the model, dynamics of g_{sw} influence dynamics of leaf transpiration rate, which in turn affects leaf water content and temperature. We simulated leaf and stem water contents, and hence the influence of capacitive water storage on hydraulic dynamics and risk, dynamically based on conservation of mass. We calculated leaf and stem (xylem) water potentials from their respective water contents and adjusted leaf and stem hydraulic conductances according to their respective vulnerability curves, assuming conductivity loss in either compartment is irreversible during a single day (unless otherwise noted). We simulated leaf temperature dynamically based on conservation of energy, using an unsteady energy balance that accounts for the buffering effect of leaf heat capacity on temperature fluctuations. We also simulated photosynthetic induction state (actual photosynthetic capacity as a fraction of its fully induced value) dynamically, assuming it changes exponentially over time toward a moving target defined by current PPFD (Taylor & Long, 2017; Salter *et al.*, 2019).

Coordination of maximum hydraulic conductance and photosynthetic capacity among leaves We assumed that maximum leaf and stem hydraulic conductances at 25°C (which are time-invariant for each leaf in our model) varied among leaf patches in proportion to the fully induced value of photosynthetic capacity at 25°C (Brodribb & Feild, 2000; Brodribb *et al.*, 2002), which in turn we assumed to be proportional to mean daily PPFD for each patch (Field, 1983).

Quantifying sunfleck dynamics To help quantify how the dynamic light environment influenced hydraulic risk, we quantified the duration and intensity of sunflecks in each PPFD time course using wavelet analysis (Figs S1, S2; Methods S2). Minimum ψ_{leaf} was negatively related to both sunfleck duration and intensity (Fig. S3a,b), though the effect of duration saturated at *c.* 30 min. The product of duration and intensity predicted $\psi_{leaf,min}$ better than either parameter alone, but with weak sensitivity (Fig. S3c). We thus computed a composite parameter, 'sunfleck strength', as log(*intensity*·minimum (*duration*, 30 min)), which predicted $\psi_{leaf,min}$ in sigmoidal fashion (Fig. S3d).

Parameter estimation Estimation of parameter values and parameter sensitivity analysis methods are described in Methods S3 and S4, respectively.

Additional model details are provided in Appendix A1.

Results

Sample dynamics of PPFD and physiology

Fig. 3 shows diurnal time courses of PPFD simulated by Helios for 12 leaf patches with a range of mean PPFD and sunfleck patterns. These and similar traces were used as forcing functions in simulations of diurnal physiology for 10 000 leaf patches. Fig. 4 shows sample results for two patches. Leaf temperature (Fig. 4a, b) follows air temperature through the day, rising periodically above it due to light absorption during sunflecks. Stomatal conductance (Fig. 4c,d) also rises during each sunfleck, lagging

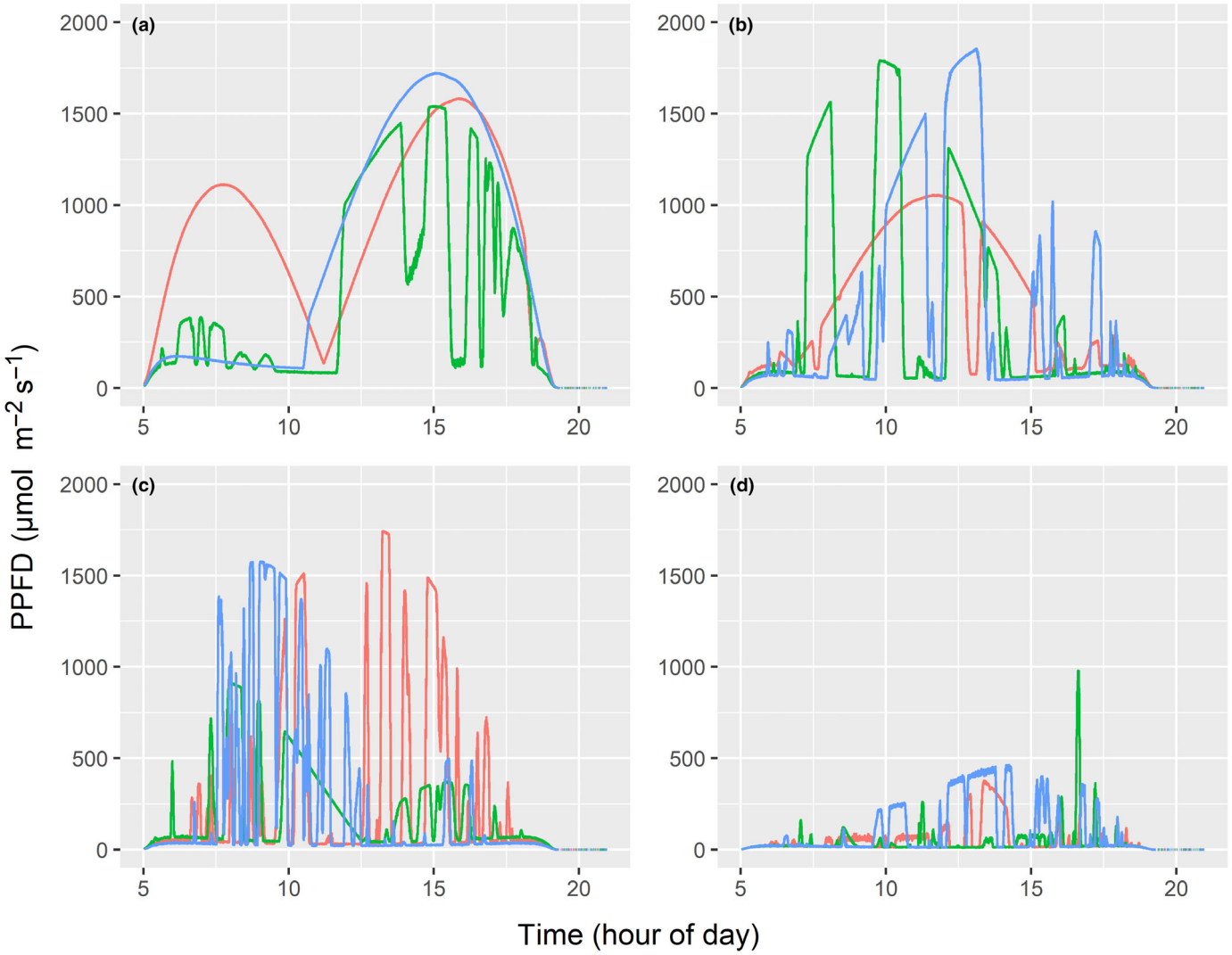

Fig. 3 Time courses of photosynthetic photon flux (PPFD) for 12 sample leaf patches, illustrating the variation in dynamic light environment simulated by Helios. Time courses are grouped by ranges of mean PPFD ((a) 472–793 μmol m^{-2} s^{-1}, (b) 358–408 μmol m^{-2} s^{-1}, (c) 178–246 μmol m^{-2} s^{-1}, (d) 36–92 μmol m^{-2} s^{-1}) and colored differently within each panel to distinguish them from one another.

behind its optimal target value. Stem and leaf water potentials (Fig. 4e,f) follow similar patterns, but vertically inverted – falling as stomatal conductance rises – and with dynamics muted by the capacitive effect of leaf and stem water contents. In both sample simulations, large sunflecks early in the day cause declines in leaf water potential sufficient to reduce leaf hydraulic conductance substantially (Fig. 4g,h); stem hydraulic conductance does not decline noticeably, because stem water potential is less negative than ψ_{leaf} and the hydraulic ψ_{50} is more negative for stems than for leaves.

Kinetic parameters influence the economic landscape of short-term hydraulic risk

To explore and quantify how transient phenomena affect hydraulic risk, we computed aggregated carbon gain (**A**) and the aggregated carbon cost of short-term hydraulic risk (C_{risk}) for 10 000 leaf patches, across a range of values for various kinetic parameters and for the parameter, ψ_{50risk}, that describes the degree of 'riskiness' of stomatal behavior. The resulting relationships between **A** and ψ_{50risk}, and between C_{risk} and ψ_{50risk}, describe the *economic landscape of short-term hydraulic risk*: that is, they show how stomatal behavior mediates the impact of hydraulic risk on carbon economy at the integrated scale of a canopy over an entire day. Our results demonstrate that kinetic parameters influence that economic landscape. For example, the effects of ψ_{50risk} on **A** and C_{risk} differ when the rate constant for adjustment of stomatal conductance via guard cell osmotic pressure (α_π, Fig. 5) is altered. **A** is maximized by less-risky stomatal behavior (a less-negative value of ψ_{50risk}) in a canopy with faster stomatal kinetics (α_π = 50% larger than the default value in Table 1) and conversely by more-risky stomatal behavior when stomata are slower (α_π = 50% smaller than the default value; Fig. 5a). Likewise, **A** is maximized by more-risky stomatal behavior in leaves with greater saturated water content (SWC), which buffers the effects of transient

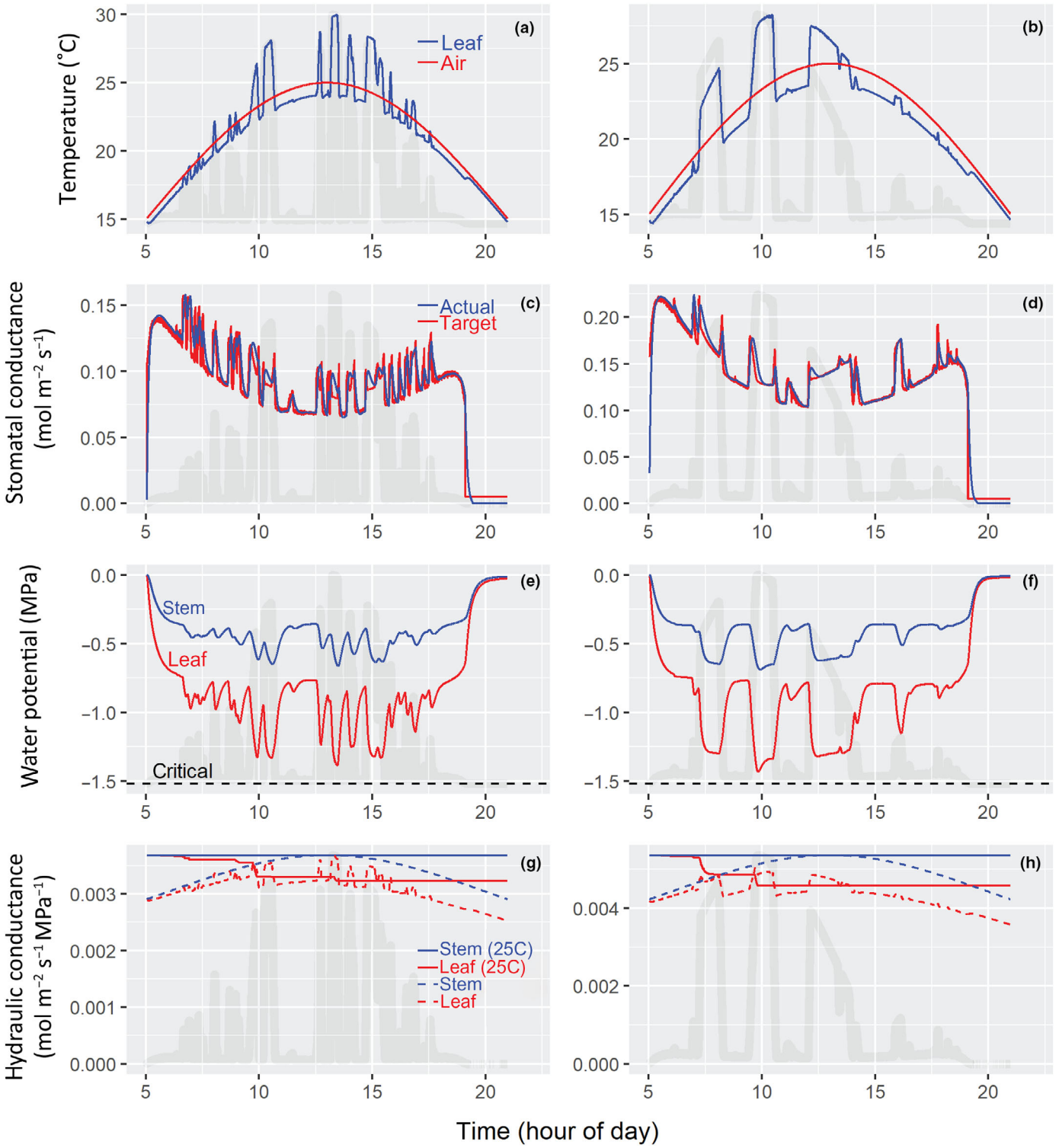

Fig. 4 Sample simulation results for two leaves. (a, b) Leaf and air temperatures; (c, d) stomatal conductance (actual simulated value (blue lines) and steady-state target value (red lines)); (e, f) water potentials of stem (blue) and leaf (red) compartments; (g, h) hydraulic conductances of stem (blue) and leaf (red) compartments. In (g, h), values corrected to 25°C (solid lines) are shown alongside actual values that include the effect of temperature (dashed lines), to highlight loss of conductivity independent of temperature. Time courses of photosynthetic photon flux (PPFD) are shown in the background for reference, with semitransparent gray lines; the PPFD time course in (a, c, e, g) here is also shown in Fig. 3(c) with a red line, and that in (b, d, f, h) is shown in Fig. 3(b) with a green line.

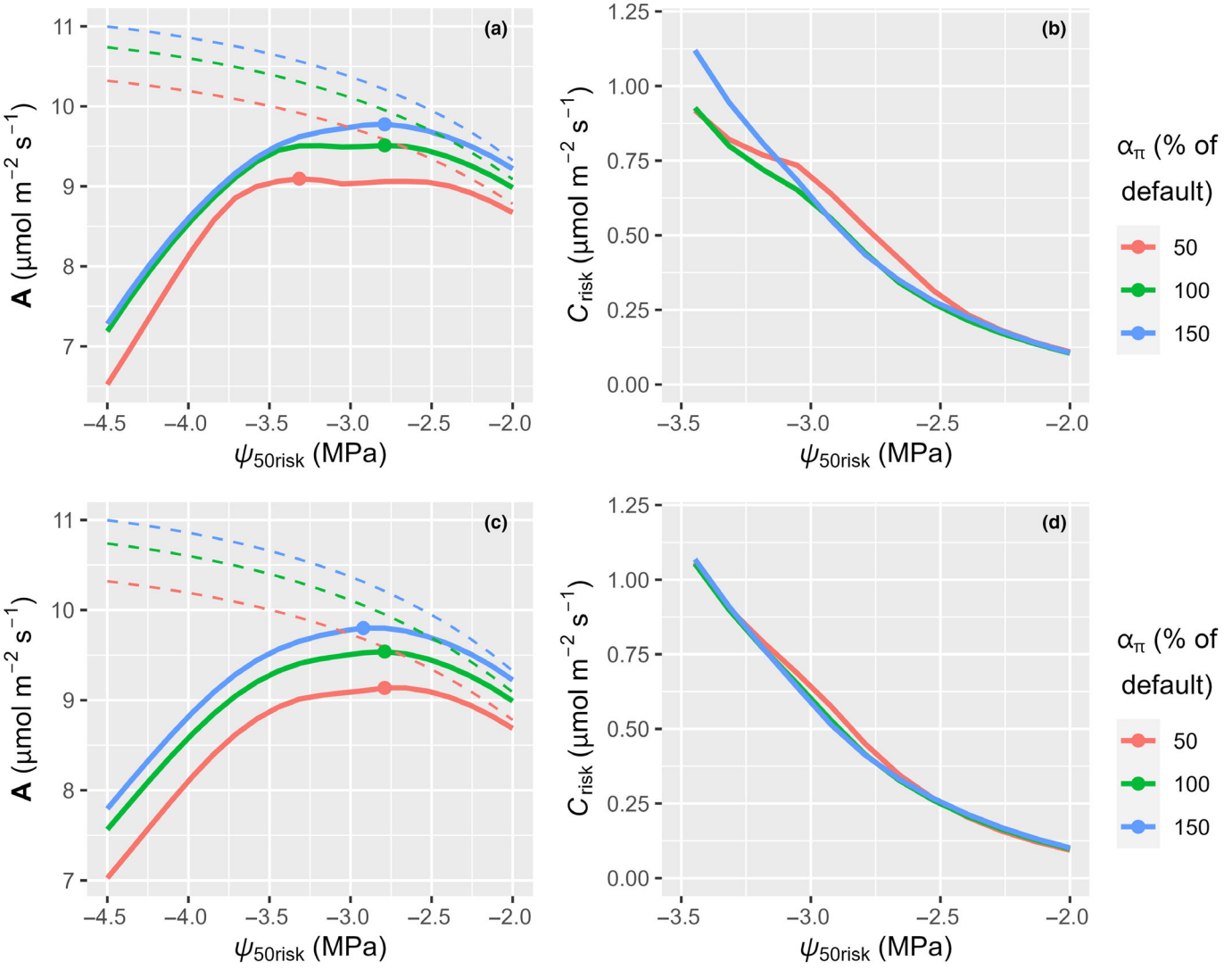

Fig. 5 Intrinsic speed of stomatal responses to the environment (α_π, the rate constant for adjustment of guard cell osmotic pressure) affects the economic landscape of short-term hydraulic risk, regardless of whether leaf hydraulic decline was assumed to be irreversible (a, b) or instantaneously reversible (c, d). (a, c) α_π influences the stomatal strategy (as gauged by the parameter ψ_{50risk}) that maximizes aggregated carbon gain (**A**, mean daily CO_2 assimilation rate across all 10 000 simulated leaf patches); the point of maximum **A** in each curve is shown with a closed circle. Dashed lines in (a, c) represent aggregated carbon gain from simulations in which hydraulic risk was omitted by setting the water potentials at which leaf and stem hydraulic conductance declined by 50% (ψ_{50leaf} and ψ_{50stem}, respectively) to −100 MPa. (b, d) α_π also influences the relationship between stomatal strategy and the aggregated carbon cost of short-term hydraulic risk (C_{risk}, the decrease in **A** caused by hydraulic risk; i.e. the difference between dashed and solid lines in (a, c)). (The *x*-axis range in (b, d) is narrower than in (a, c), to focus on the range of ψ_{50risk} in which the maximum in **A** occurs.)

fluctuations in gas exchange on leaf water potential and hence hydraulic conductance (Fig. 6a). Kinetic parameters also influence how stomatal behavior affects the carbon cost of hydraulic risk: C_{risk} increases as stomatal behavior becomes more risky (as ψ_{50risk} declines), but the exact shape of that relationship depends on kinetic parameters (Figs 5b, 6b). For example, for ψ_{50risk} between *c.* −2.4 and −3.1 MPa, C_{risk} is greatest for 'slow' stomata, whereas for ψ_{50risk} below −3.3 MPa, C_{risk} is greatest for 'fast' stomata (Fig. 5b). Similarly, the effect of differences in leaf-saturated water content on C_{risk} is greater at intermediate ψ_{50risk}, peaking at *c.* −3.1 MPa, than at more negative ψ_{50risk} (Fig. 6b). In contrast to α_π and leaf SWC, the rate constant for photosynthetic induction (α_V) had very small effects on the economic landscape of short-term hydraulic risk (Fig. S4).

Effects of kinetics on the economics of hydraulic risk persisted, but were quantitatively different, in simulations that assumed K_{leaf} decline was instantaneously reversible (Figs 5c,d, 6c,d). With reversible K_{leaf} decline, α_π had weaker effects on the value of ψ_{50risk} that maximized **A** (Fig. 5c), whereas SWC had slightly stronger effects (Fig. 6c). Shifts in kinetic parameters led to clear changes in the relationship between stomatal strategy and the carbon cost of hydraulic risk, regardless of the reversibility of K_{leaf} decline (Fig. 7).

To visualize the effect of kinetic parameters on physiological kinetics, we simulated responses of stomatal conductance, leaf

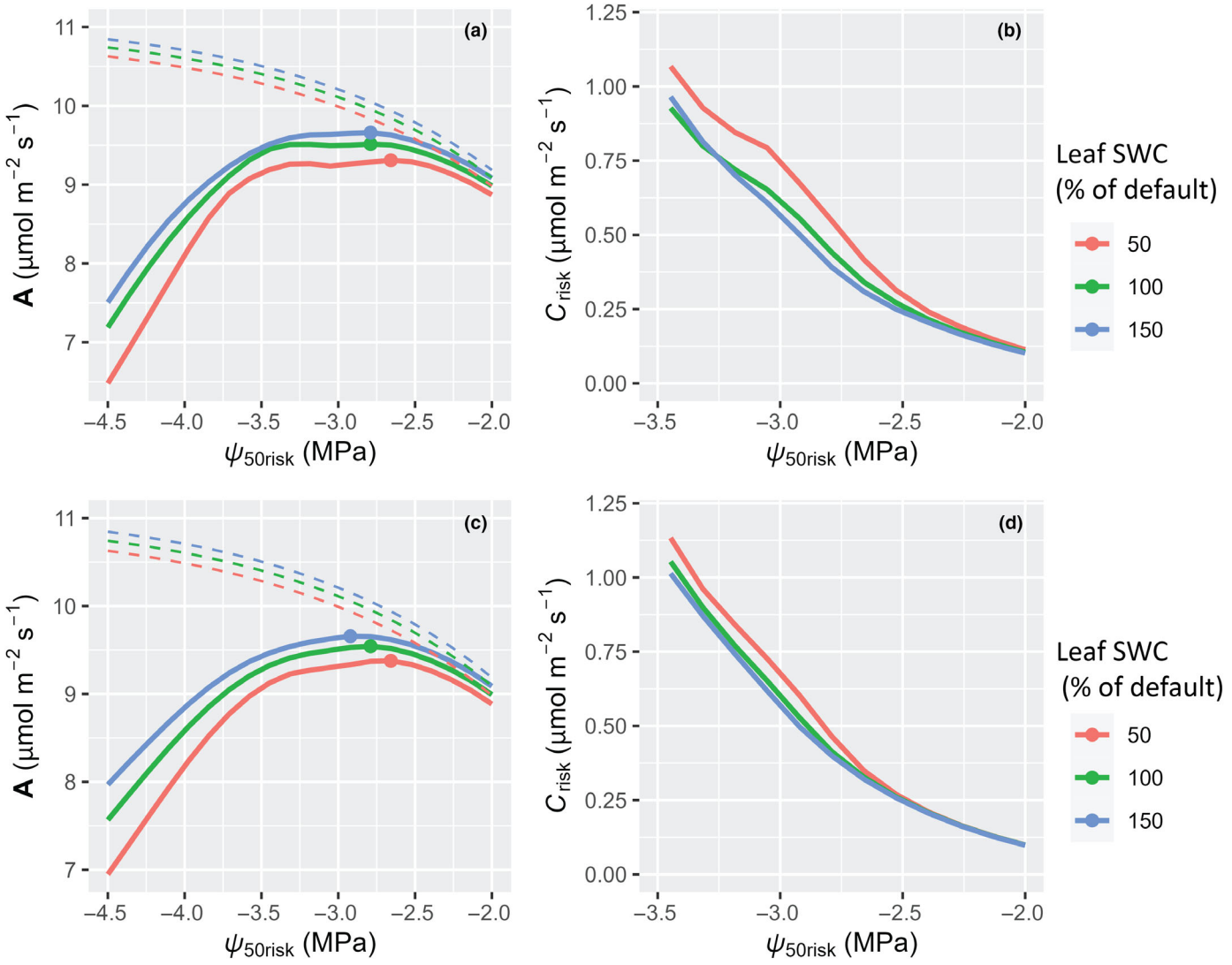

Fig. 6 Because leaf water stores can act as a buffer to mute transient dynamics of leaf water potential, leaf-saturated water content (SWC or $n_{leaf,max}$) affects the economic landscape of short-term hydraulic risk, whether leaf hydraulic decline is assumed to be irreversible (a, b) or instantaneously reversible (c, d). (a, c) Leaf SWC influences the stomatal strategy (as gauged by the water potential at which the penalty function reaches 0.5 (50%), ψ_{50risk}) that maximizes aggregated carbon gain (**A**, mean daily carbon gain across all 10 000 simulated leaf patches); the point of maximum **A** in each curve is shown with a closed circle. Dashed lines in (a, c) represent aggregated carbon gain from simulations in which hydraulic risk was omitted by setting the water potentials at which leaf and stem hydraulic conductance declined by 50% (ψ_{50leaf} and ψ_{50stem}, respectively) to −100 MPa. (b, d) Leaf SWC also influences the relationship between stomatal strategy and the aggregated carbon cost of short-term hydraulic risk (C_{risk}, the decrease in **A** caused by hydraulic risk; i.e. the difference between dashed and solid lines in (a, c)). (The *x*-axis range in (b, d) is narrower than in (a, c), to focus on the range of ψ_{50risk} in which the maximum in **A** occurs.)

water potential, and temperature to a discrete increase in PPFD from 100 to 1600 μmol m^{-2} s^{-1}, for each of the three values of α_π and SWC discussed above (Fig. S5). The effect of α_π on g_{sw} dynamics was greatest for 'slow' vs 'normal' stomata (Fig. S5a); by contrast, the effect of SWC on leaf water potential dynamics was similar for 'slow' (high SWC) vs 'normal' and for 'normal' vs 'fast' (Fig. S5d).

Sunfleck strength influences the economics of short-term hydraulic risk

Sunfleck strength influenced both **A** and C_{risk}. For example, **A** was maximized by more-conservative stomatal strategies (less-negative ψ_{50risk}) in leaf patches with the strongest sunflecks and conversely by more-risky strategies in patches with weak sunflecks (Fig. 8a). Likewise, C_{risk} was generally greater in leaf patches with stronger peak sunflecks (Fig. 8b).

Canopy structure slightly alters the economics of short-term 'hydraulic risk'

The simulations described above used Helios output for a spatially homogeneous canopy with a spherical LAD. To assess the impact of aggregation of leaves into individual tree crowns and the influence of varying LAD, we performed additional simulations using Helios output for canopies with spherically

aggregated crowns and either spherical (isotropic), planophile (mostly horizontal), or erectophile (mostly vertical) LADs. Values of ψ_{50risk} that maximized **A** were strongly positively related to peak sunfleck strength across cohorts differing in mean daily PPFD (Fig. S6a), but the shape of the relationship differed somewhat in heterogeneous crowns with different LADs (Fig S6b–d); for example, peak sunfleck strength was generally smaller in heterogeneous crowns, particularly for leaf patches with intermediate PPFD. Much of the difference between the homogeneous canopy simulation and those with heterogeneous canopies may be attributable to the greater leaf area density used in the latter.

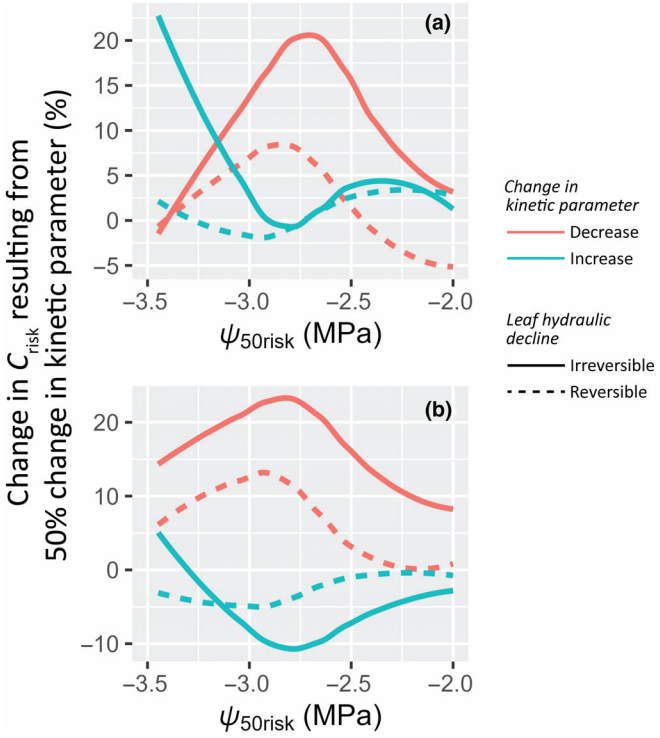

Fig. 7 Changes in kinetic parameters alter the relationship between the carbon cost of hydraulic risk (C_{risk}) and stomatal strategy (ψ_{50risk}), irrespective of the reversibility of leaf hydraulic decline. Shown here are % differences in C_{risk} caused by changes in kinetic parameters (a, stomatal speed, α_π; b, leaf-saturated water content, SWC). α_π or SWC was reduced (red) or increased (blue) by 50% compared with its default value; leaf hydraulic decline was assumed irreversible (solid lines) or reversible (dashed lines).

Soil water potential influences the economics of short-term hydraulic risk

Decreasing ψ_{soil} from 0 to −1.8 MPa greatly reduced **A** and increased C_{risk} for any stomatal strategy (Fig 9a,b). The stomatal strategy that maximized **A** was somewhat more risky under slight soil drought (**A** was maximized by $\psi_{50risk} = -3.2$ MPa at $\psi_{soil} = -0.2$ MPa, vs by $\psi_{50risk} = -2.8$ MPa at $\psi_{soil} = 0$), but further reduction in ψ_{soil} favored less-risky stomatal strategies (Fig. 9a; e.g. **A** was maximized by $\psi_{50risk} = -2.4$ MPa at $\psi_{soil} = -1.8$ MPa).

Transient dynamics amplify loss of hydraulic conductivity during a sunfleck

To illustrate how transient dynamics of gas exchange, which depend on kinetic parameters, influence hydraulic risk, we examine an example in which transient phenomena cause leaf water potential to decline below its eventual steady-state value during a sunfleck. Fig. S7 shows a close-up view of a large sunfleck from *c.* 09:30 to 10:30 h (this is the same sunfleck shown in Fig 4b,d,f,h). As PPFD increases, both evaporative demand and photosynthetic induction state increase (Fig. S7a, blue and black lines). Their effects on the optimal target value of g_{sw} mostly cancel out after the peak PPFD has been reached

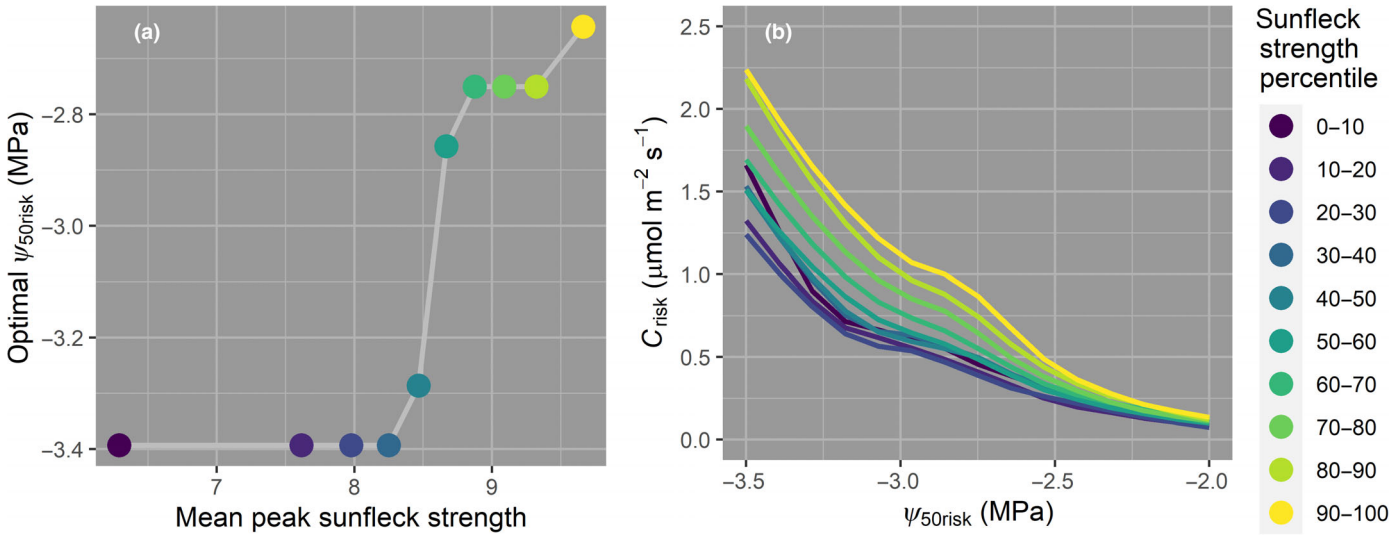

Fig. 8 Sunfleck strength influences the economic landscape of short-term hydraulic risk. (a) The stomatal strategy (represented by the water potential causing 50% penalty, ψ_{50risk}) that maximizes aggregated carbon gain is more conservative (ψ_{50risk} is less negative) in leaves with stronger peak sunflecks, and (b) the aggregated carbon cost of short-term hydraulic risk (C_{risk}) is generally greater in leaves with stronger peak sunflecks. Colors = mean peak sunfleck strength within cohorts of 1000 leaf patches (cohorts defined by percentiles of sunfleck strength). Leaf hydraulic decline was irreversible in these simulations.

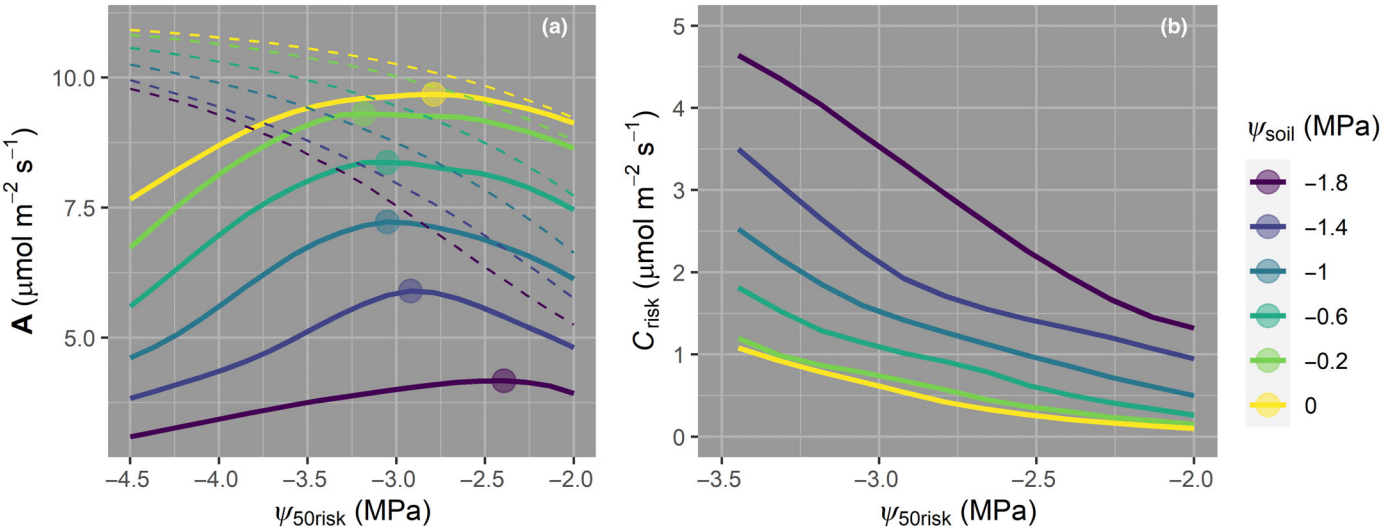

Fig. 9 Soil water potential (ψ_{soil}) influences the economic landscape of short-term hydraulic risk. (a) As ψ_{soil} declines, aggregated carbon gain (**A**, mean daily carbon gain across all 10 000 simulated leaf patches) decreases, and the stomatal strategy (as gauged by the parameter ψ_{50risk}) that maximizes **A** also shifts; the point of maximum **A** in each curve is shown with a colored symbol. Dashed lines in (a) represent aggregated carbon gain from simulations in which hydraulic risk was omitted by setting ψ_{50leaf} and ψ_{50stem} to −100 MPa. (b) Decreasing ψ_{soil} increases the aggregated carbon cost of short-term hydraulic risk (C_{risk}, the decrease in **A** caused by hydraulic risk; i.e. the difference between dashed and solid lines in (a)) and also changes the shape of the relationship between stomatal strategy and C_{risk}. Leaf hydraulic decline was irreversible in these simulations.

(red line in Fig. S7d). However, g_{sw} is controlled not only by guard cell osmotic pressure (π_g; solid black line in Fig. S7b), which is actively regulated to seek the optimal target g_{sw}, but also by the effect of leaf water potential (Fig. S7c, red line) on guard cell and epidermal turgor pressures (Fig. S7b; red and blue lines, respectively). As ψ_{leaf} declines, the resulting drop in epidermal backpressure transiently increases g_{sw} (dashed black line in Fig. S7b) even as π_g is declining. As a result, transpiration rate transiently overshoots its eventual steady-state value (Fig. S7a, red line) – causing a decline in ψ_{leaf} that briefly becomes self-amplifying due to an associated decline in hydraulic conductance (increase in PLC; dashed black line in Fig. S7a). PLC only stops increasing after stomatal conductance and transpiration rate have declined (at *c.* 9:50).

Transient dynamics mediate the impact of stomatal strategy on carbon economy at the diurnal scale

In the example described above, nonsteady-state dynamics caused a greater decline in ψ_{leaf}, and thus in K_{leaf}, than would have occurred in the absence of transient phenomena. Simulating more 'risky' stomatal behavior by setting ψ_{50risk} to more negative values leads to greater stomatal conductance and hence carbon gain, but also lower minimum ψ_{leaf} and greater conductivity loss (PLC; Fig. S8a,b). The net effect of ψ_{50risk} on carbon gain integrated over the sunfleck and, on PLC at the end of the sunfleck, depends on a trade-off between greater gas exchange early in the sunfleck – including a higher transient peak – and lower gas exchange later in the sunfleck (Fig. S8a,c). This illustrates explicitly how transient phenomena, and hence kinetic parameters, influence the pattern of stomatal behavior that maximizes total carbon gain.

Sensitivity analysis

Adjustment of plant-related parameters between 75% and 125% of their default values caused small changes in **A** and mean daily minimum leaf water potential across 500 randomly selected leaf patches (Figs S9–S11). The most influential parameter was $K_{leaf25max}$, whose sensitivity coefficient (% change in dependent variable per 1% change in parameter) was 0.14% for A and 0.11% for $\psi_{leaf,min}$, respectively (Fig. S11). Most environmental parameters had little effect (Fig. S12); the largest sensitivity coefficients were 0.32% for T_{airmax} vs $\psi_{leaf,min}$ and 0.75% for c_a vs A. Varying epidermal mechanical advantage between 0 and 4 increased **A** by *c.* 10% and reduced $\psi_{leaf,min}$ by *c.* 40% (Fig. S13).

Discussion

The hydraulic penalty (HP) paradigm for stomatal modeling (Wolf *et al.*, 2016; Sperry *et al.*, 2017; Eller *et al.*, 2018, 2020; Wang *et al.*, 2020) has advanced practical prediction of stomatal conductance from optimization theory. Most HP models penalize excessive stomatal opening using the hydraulic vulnerability curve, or quantities derived from it. We hypothesized that the economic landscape of short-term hydraulic risk is also influenced by nonsteady-state processes mediated by physiological kinetics and the dynamical light environment. Our results confirmed this hypothesis by demonstrating that kinetic parameters modify the effect of stomatal strategy on the carbon cost of short-term hydraulic risk (C_{risk}) and carbon gain (**A**), aggregated over a day and over a canopy. For example, leaves with greater water storage capacity achieved maximum **A** with a more-risky stomatal strategy (Fig. 6), because water storage can buffer transient fluctuations in water potential and thereby reduce the risk of diurnal

hydraulic decline – particularly for leaf hydraulic conductance (Brodribb & Holbrook, 2003, 2004; Guyot *et al.*, 2012; Hernandez-Santana *et al.*, 2016), as leaf water potential is likely far more dynamic than stem water potential, given the large stem water stores often available in trees (Cermak *et al.*, 2007). The impact of kinetic properties on hydraulic risk was altered, but not eliminated, if we assumed K_{leaf} decline was immediately reversible, rather than irreversible. Similarly, leaves that experienced stronger sunflecks gained more carbon, in the aggregate, under a more-conservative (less risky) stomatal strategy, largely because sunfleck strength increased the carbon cost of hydraulic risk (Fig. 8).

Instantaneous shadow costs vs aggregated carbon costs

HP models assume stomatal behavior is 'optimal' if it maximizes carbon gain minus the costs of hydraulic risk. A *tacit* assumption of most HP models is that those costs are accurately represented by a penalty function (Θ) defined solely by the hydraulic vulnerability curve. But, what is Θ and how should it be formulated? Wang *et al.* (2020) note that Θ is a 'shadow cost' – a cost that is hard to compute but is nonetheless real, and commensurable with carbon gain. In other words, Θ must represent *real carbon costs* in some way, at some scale of aggregation. The reason HP models express those costs as a shadow cost, instead of simply computing them from a mechanistic model, like photosynthesis, is that the costs depend on future contingencies and therefore cannot be entirely computed from current instantaneous conditions (the costs of embolism repair may be computable, but are poorly constrained; Zwieniecki & Holbrook, 2009). For a leaf that is trying to choose the best value of stomatal conductance for the next moment in time, the prospect that its future carbon gain may be reduced by hydraulic decline is not predicted by the current instantaneous value of A in the HP goal function. In economic terms, that prospect is an *externality* to A. The purpose of Θ is to capture such externalities, which only manifest as real, computable carbon costs when gas exchange is integrated over a long time frame and over many leaves. (If it were practical to simply write down an equation for that aggregated carbon gain as a function of stomatal conductance, we would not need the mysterious 'shadow cost' formulation.) A truly 'optimal' formulation of Θ would be one that maximizes net carbon gain at such an aggregated scale.

The rationale behind our approach was to perform part of that aggregation by brute force, by integrating over a day for many leaves. Our measure of aggregated carbon gain (**A**) thus includes externalities that are not captured by the instantaneous value of A in the goal function, and which therefore represent part of Θ. Importantly, we have not identified the truly optimal formulation of Θ, because computational constraints prevented us from integrating beyond a single day. Other important risks manifest only at longer time scales, such as mortality during sustained drought and the cost of replacing tissues that succumb to total hydraulic failure. Nonetheless, because we have shown that kinetic factors influence the short-term component of the carbon cost of hydraulic risk, it follows that broader, longer-term measures of those costs must also be influenced by kinetic factors. (Longer-term processes could somehow exactly cancel out the effects of kinetics on short-term risk, but that seems unlikely.) Therefore, we conclude that current formulations of Θ are incomplete and should be relaxed to accommodate kinetic factors.

Empirical accuracy vs theoretical coherence

This study concerns a purely theoretical question: do HP models that ignore kinetic properties truly represent the optimization hypothesis? Our results suggest they cannot. A completely different, *empirical* question is whether HP models accurately predict actual stomatal behavior, and whether including kinetic properties would improve their predictions. Evidence suggests HP models predict stomatal behavior well, at least qualitatively (e.g. Eller *et al.*, 2020; Wang *et al.*, 2020; Bassiouni & Vico, 2021). However, one study has shown that basing penalty functions explicitly on hydraulics did not improve predictive accuracy (Bassiouni & Vico, 2021). Other evidence points in the same direction. Penalty function parameters calibrated to produce the best fit between predicted and observed productivity differed systematically from hydraulic vulnerability parameters, across a range of functional types (Eller *et al.*, 2020), namely best-fit penalty functions were less 'risky' than hydraulic penalty functions (Fig. S14). Wang *et al.* (2020) also conducted an empirical test of HP models, including a new model they proposed in which $\Theta = E/E_c$ (the ratio of transpiration rate to its value at the critical water potential for catastrophic xylem failure). Unfortunately, they reported only mean absolute percentage prediction errors for each model, so we cannot infer whether their model would be more accurate if Θ were modified to account for kinetic factors.

It is unsurprising that vulnerability curve parameters alone cannot fully predict stomatal behavior, given that some species close their stomata at water potentials far above the threshold for catastrophic xylem failure, while others more closely approach the threshold (Klein, 2014; Anderegg *et al.*, 2016; Bartlett *et al.*, 2016; Meinzer *et al.*, 2017; Pivovaroff *et al.*, 2018; Chen *et al.*, 2019; Li *et al.*, 2019). Such differences may arise, at least in part, from effects of kinetic factors of physiology and the dynamical light environment on the economics of hydraulic risk. The HP modeling paradigm cannot, by design, predict large differences in safety margin unless the penalty function is relaxed to account for such factors. However, the flexibility needed to accommodate kinetic factors would not necessarily cause predictions to diverge wildly from observations. For example, because stomata usually close before substantial xylem hydraulic decline occurs, leaf water potential usually remains above thresholds for catastrophic xylem failure, except during sustained drought that causes maximal stomatal closure (Bartlett *et al.*, 2016; Martin-StPaul *et al.*, 2017; Creek *et al.*, 2020). Our simulations predicted a similar outcome: leaf water potential remained above the threshold for stem xylem failure in all 10 000 leaf patches even when ψ_{50risk} was decoupled from the hydraulic ψ_{50} for whole-plant water transport ($\psi_{50plant}$) and set to much more negative values (Fig. 10).

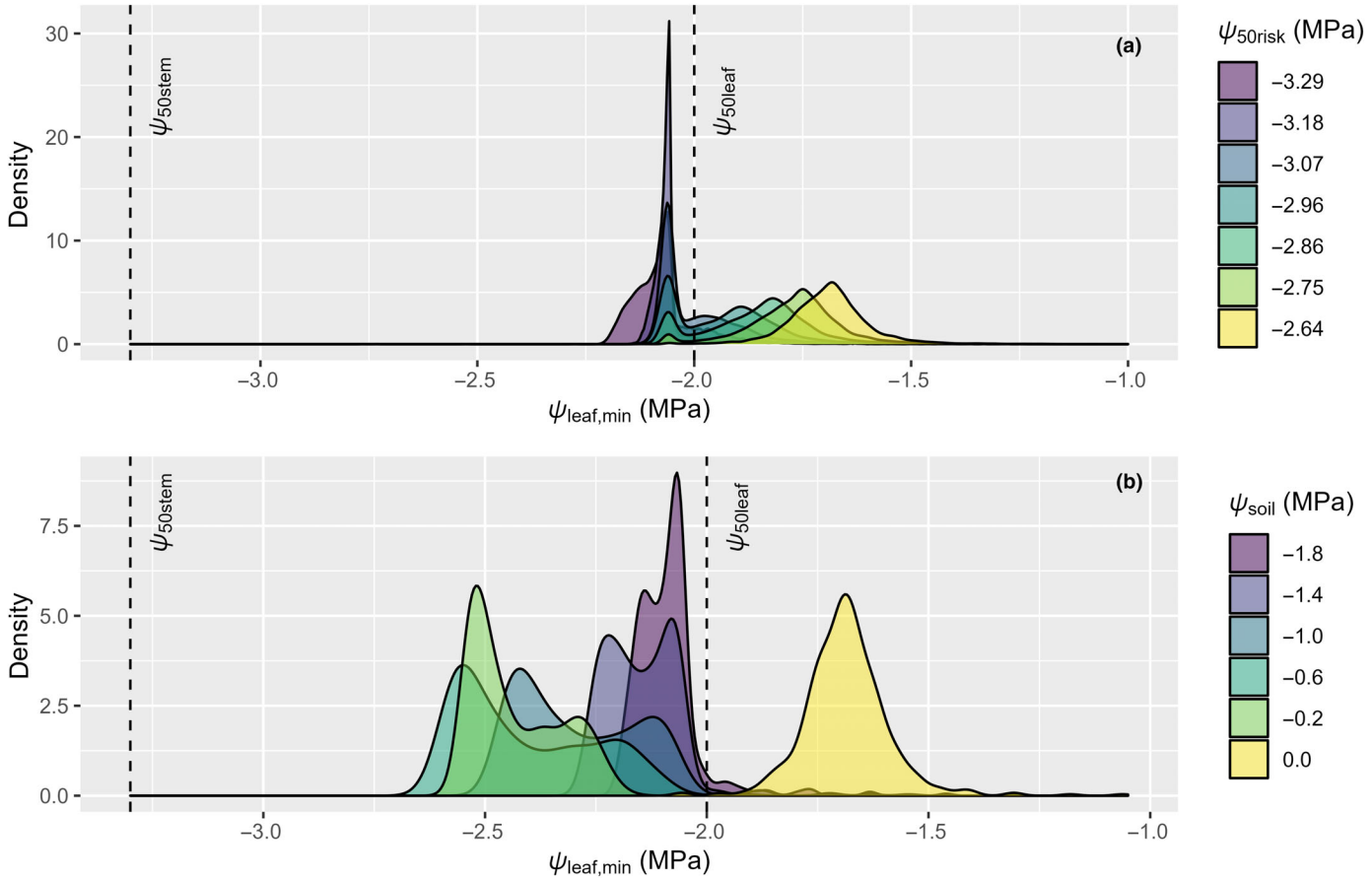

Fig. 10 Minimum daily leaf water potential ($\psi_{leaf,min}$) in all simulated leaf patches remained far above the water potential causing 50% loss of stem hydraulic conductance (ψ_{50stem}, −3.3 MPa), (a) even for stomatal strategies in which the water potential causing 50% penalty in the goal function for optimal stomatal conductance (ψ_{50risk}) was quite low and nearly equal to ψ_{50stem}, and (b) even when soil water potential was reduced (and ψ_{50risk} was set at the value that maximized **A** at each soil water potential (ψ_{soil}), as shown in Fig. 9). In (a), distributions of $\psi_{leaf,min}$ are shown for simulations using values of ψ_{50risk} spanning the range of values that maximized aggregated carbon gain for different values of kinetic parameters in Figs 5 and 6. Simulations in (a) used 10 000 leaf patches; those in (b) used 500 leaf patches.

In light of our results, we suggest that the usefulness of the HP paradigm would benefit from a systematic evaluation of (1) whether its predictions deviate systematically from observations across species, as suggested by the study discussed earlier (Eller *et al.*, 2020; Fig. S13), and (2) whether such deviations are associated with differences in kinetic factors that influence hydraulic risk. For example, our findings suggest that the optimal stomatal strategy should be less risk-averse in species with slower stomatal responses or greater saturated leaf water content, all else equal (cf. Figs 5, 6). More generally, we suggest that there is no rational basis to assume that ψ_{50}-based hydraulic penalties generate stomatal behavior that actually optimizes the trade-off between carbon gain and hydraulic risk. We agree that the 'truly optimal' penalty function probably looks a lot like the hydraulic vulnerability curve: that is, the water potential scale of stomatal closure should be *correlated* with ψ_{50}, and the penalty should increase ever more steeply as water potential becomes more negative. But, we do not believe it has been shown that the truly optimal penalty function *is simply the hydraulic vulnerability curve itself* (nor another function derived from it, as in the model of Wang *et al.*, 2020). A first step toward generalizing HP models would be to augment the penalty function with an empirically tunable parameter. For example, for the Eller model, the penalty function might change as follows:

$$\Theta(\text{original}) = A \cdot \frac{|\psi_{leaf}|^{\xi}}{|\psi_{50}|^{\xi} + |\psi_{leaf}|^{\xi}} \rightarrow \Theta(\text{new}) = A \cdot \frac{|\psi_{leaf}|^{\xi}}{|\psi_{50} + \delta|^{\xi} + |\psi_{leaf}|^{\xi}} \quad \text{Eqn 3}$$

The new parameter δ could be tuned to optimize the resulting predictions: δ would be positive for species whose stomata behave more conservatively than predicted by the original goal function, or negative for species with more-risky behavior. A benefit of this approach is that all of the factors that influence hydraulic risk other than the vulnerability curve itself would be distilled into a single parameter, δ, which would facilitate analysis of those factors and their ecological and environmental correlates. A similar alternative is to have δ be multiplicative, rather than additive, with ψ_{50}.

Sunflecks drive hydraulic risk

We found that the economic landscape of short-term hydraulic risk was strongly influenced by the strength of sunflecks, which drive transient increases in water loss. In our simulations, leaves that experienced stronger peak sunflecks generally achieved maximal **A** with a more-conservative stomatal strategy (less-negative ψ_{50risk}; Fig. 8). Sunfleck strength also largely mediated differences in the economics of short-term risk between leaves in different light environments: **A** was maximized by more-conservative stomatal behavior for leaves of intermediate mean PPFD, which also had stronger sunflecks (Fig. S6). Canopy structure and LAD had weak effects: clumping of leaves into dense crowns reduced peak sunfleck strength somewhat but had little effect on the stomatal strategy that maximized **A** (Fig. S6).

Stomatal kinetics: a speed vs safety trade-off?

Our simulations predicted that a plant with fast stomatal kinetics will gain more carbon over a day under a more-conservative stomatal strategy. By contrast, we had suspected that leaves with faster stomata could close more rapidly to prevent hydraulic failure and would therefore be less likely to suffer negative consequences of less-conservative behavior. Faster stomatal opening may, however, enhance hydraulic risk by increasing peak transpiration rate during a sunfleck. Lawson & Vialet-Chabrand (2018) concluded that slow stomatal responses can improve average water use efficiency, albeit at the cost of reduced carbon gain. We similarly found that, for a given stomatal strategy, leaves with slower stomata gained less carbon over the day than leaves with faster stomata (Fig. 5a). Optimal stomatal kinetics may thus depend on a trade-off between increased photosynthesis and reduced hydraulic risk. Fast stomatal responses may themselves also be inherently more costly than slow responses (Vico *et al.*, 2011), although the energetic costs are difficult to quantify (Lawson & Blatt, 2014), and any such costs are likely greatly outweighed by the resulting gains (Papanatsiou *et al.*, 2019). More generally, the effects of sunfleck properties and physiological kinetics on the economics of short-term hydraulic risk argue strongly that stomatal behavior cannot be understood without considering nonsteady-state phenomena. One major reason stomata must maintain a safety margin between ψ_{leaf} and ψ_c (Sperry, 2004; Meinzer *et al.*, 2009; Johnson *et al.*, 2011), in addition to hedging against the risk of desiccation during sustained drought (Mäkelä *et al.*, 1996), is to prevent excursions below ψ_c during unpredictable transient spikes in transpiration rate caused by sunflecks. This suggests dynamical phenomena are fundamental in defining what pattern of stomatal behavior is optimal.

Limitations of our approach

Our results are based entirely on simulations; direct measurements are infeasible at the scale and density needed to infer the economic landscape of short-term hydraulic risk for an entire canopy. Some elements of our model may thus limit the generality of our conclusions. (1) Our sunfleck simulations assumed rigid leaves; in reality, high-frequency motion caused by wind may dampen sunfleck intensity, reducing hydraulic risk (Pearcy, 1990; Burgess *et al.*, 2021). Turbulence may also rapidly deliver packets of dry air deep in the canopy (Bailey & Stoll, 2016); we assumed vapor pressure was constant over the day. (2) We simulated physiological dynamics for the smallest leaf elements resolved by Helios (1 cm × 1 cm patches), rather than for entire leaves (5 cm × 5 cm); this ignores potential interactions between stomata in different regions of a leaf exposed to different PPFD (Buckley & Mott, 2000). (3) We compared stomatal strategies by varying one parameter of the penalty function (ψ_{50risk}). Future work should also vary the steepness parameter (ξ), and examine different penalty functions altogether. (4) As noted earlier, we did not examine the influence of long-term risk posed by extended drought (Lu *et al.*, 2016, 2020; Martin-StPaul *et al.*, 2017). However, accounting for long-term risk should not change the general conclusion that the economics of stomatal function depends on dynamic features of the light environment and leaf physiology; indeed, our results align with the general conclusions of Lu *et al.* (2016, 2020) and Martin-StPaul *et al.* (2017) in showing that optimal stomatal behavior is partly defined by stochastic dynamics in the environment.

Conclusion

We used diurnal simulations of physiology in 10 000 leaf patches within a canopy to infer whether the economic landscape of short-term hydraulic risk is influenced by physiological kinetics and dynamics of PPFD. Our results show that the influence of stomatal behavior on aggregated carbon gain and the aggregated carbon cost of short-term hydraulic risk depends on stomatal response speed, the buffering effect of leaf water storage, the strength of sunflecks, and soil water potential, but minimally on photosynthetic induction speed. These results suggest the penalty function in HP models should be modified to account for kinetic factors, which would better represent the optimization hypothesis while capturing a degree of parametric freedom that may help to represent diversity in stomatal strategies across species and environments.

Acknowledgements

This work was supported by the National Science Foundation (award nos. 1557906, 1951244, and 2047628) and the USDA National Institute of Food and Agriculture (Hatch projects 1016439 and 1013396, award nos. 2020-67013-30913 and 2020-38420-30728). TNB thanks Aaron Potkay and Lawren Sack for illuminating discussions during the development of this work. We also thank several anonymous referees and Professor Belinda Medlyn for constructive criticism that greatly clarified the nature and proper conclusions of our analysis.

Competing interests

None declared.

Author contributions

TNB conceived and designed the study in consultation with EHF and BNB, conducted the physiological simulations and most of the analysis, and drafted the paper. BNB and EHF conducted the canopy light penetration simulations. EHF analyzed the effect of canopy structure. All authors edited the text.

ORCID

Brian N. Bailey https://orcid.org/0000-0003-1919-2324
Thomas N. Buckley https://orcid.org/0000-0001-7610-7136
Ethan H. Frehner https://orcid.org/0000-0002-0039-8421

Data availability

This study presents no new data. Code for Helios is available at https://github.com/PlantSimulationLab/Helios. JULIA code for physiological simulations is available at https://github.com/TomBuckleyLab/RiskNP2023 and is also published with this article as Methods S6.

References

Anderegg WR, Flint A, Huang C, Flint L, Berry JA, Davis FW, Sperry JS, Field CB. 2015. Tree mortality predicted from drought-induced vascular damage. *Nature Geoscience* **8**: 367–371.

Anderegg WR, Klein T, Bartlett M, Sack L, Pellegrini AF, Choat B, Jansen S. 2016. Meta-analysis reveals that hydraulic traits explain cross-species patterns of drought-induced tree mortality across the globe. *Proceedings of the National Academy of Sciences, USA* **113**: 5024–5029.

Bailey BN. 2018. A reverse ray-tracing method for modelling the net radiative flux in leaf-resolving plant canopy simulations. *Ecological Modelling* **368**: 233–245.

Bailey BN. 2019. Helios: A scalable 3D plant and environmental biophysical modeling framework. *Frontiers in Plant Science* **10**: 1185.

Bailey BN, Stoll R. 2016. The creation and evolution of coherent structures in plant canopy flows and their role in turbulent transport. *Journal of Fluid Mechanics* **789**: 425–460.

Ball JT, Woodrow IE, Berry JA. 1987. A model predicting stomatal conductance and its contribution to the control of photosynthesis under different environmental conditions. In: Biggens J, ed. *Progress in photosynthesis research.* Leiden, the Netherlands: Martinus Nijhoff, 221–224.

Bartlett MK, Klein T, Jansen S, Choat B, Sack L. 2016. The correlations and sequence of plant stomatal, hydraulic, and wilting responses to drought. *Proceedings of the National Academy of Sciences, USA* **113**: 13098–13103.

Bassiouni M, Vico G. 2021. Parsimony vs predictive and functional performance of three stomatal optimization principles in a big-leaf framework. *New Phytologist* **231**: 586–600.

Bonan GB. 2008. Forests and climate change: forcings, feedbacks, and the climate benefits of forests. *Science* **320**: 1444–1449.

Brodersen C, McElrone A. 2013. Maintenance of xylem network transport capacity: a review of embolism repair in vascular plants. *Frontiers in Plant Science* **4**: 108.

Brodribb TJ, Feild TS. 2000. Stem hydraulic supply is linked to leaf photosynthetic capacity: evidence from New Caledonian and Tasmanian rainforests. *Plant, Cell & Environment* **23**: 1381–1388.

Brodribb TJ, Holbrook NM. 2003. Stomatal closure during leaf dehydration, correlation with other leaf physiological traits. *Plant Physiology* **132**: 2166–2173.

Brodribb TJ, Holbrook NM. 2004. Diurnal depression of leaf hydraulic conductance in a tropical tree species. *Plant, Cell & Environment* **27**: 820–827.

Brodribb TJ, Holbrook NM, Gutierrez MV. 2002. Hydraulic and photosynthetic coordination in seasonally dry tropical forest trees. *Plant, Cell & Environment* **25**: 1435–1444.

Brutsaert W. 1975. On a derivable formula for long-wave radiation from clear skies. *Water Resources Research* **11**: 742–744.

Buckley TN. 2017. Modeling stomatal conductance. *Plant Physiology* **174**: 572–582.

Buckley TN, Mott KA. 2000. Stomatal responses to non-local changes in PFD: evidence for long-distance hydraulic interactions. *Plant, Cell & Environment* **23**: 301–309.

Buckley TN, Mott KA. 2002. Dynamics of stomatal water relations during the humidity response: implications of two hypothetical mechanisms. *Plant, Cell & Environment* **25**: 407–419.

Buckley TN, Mott KA, Farquhar GD. 2003. A hydromechanical and biochemical model of stomatal conductance. *Plant, Cell & Environment* **26**: 1767–1785.

Buckley TN, Sack L, Farquhar GD. 2017. Optimal plant water economy. *Plant, Cell & Environment* **40**: 881–896.

Buckley TN, Sack L, Gilbert ME. 2011. The role of bundle sheath extensions and life form in stomatal responses to leaf water status. *Plant Physiology* **156**: 962–973.

Burgess AJ, Durand M, Gibbs JA, Retkute R, Robson TM, Murchie EH. 2021. The effect of canopy architecture on the patterning of "windflecks" within a wheat canopy. *Plant, Cell & Environment* **21**: 589–598.

Cermak J, Kucera J, Bauerle WL, Phillips N, Hinckley TM. 2007. Tree water storage and its diurnal dynamics related to sap flow and changes in stem volume in old-growth Douglas-fir trees. *Tree Physiology* **27**: 181–198.

Chen Z, Li S, Luan J, Zhang Y, Zhu S, Wan X, Liu S. 2019. Prediction of temperate broadleaf tree species mortality in arid limestone habitats with stomatal safety margins. *Tree Physiology* **39**: 1428–1437.

Choat B, Brodribb TJ, Brodersen CR, Duursma RA, López R, Medlyn BE. 2018. Triggers of tree mortality under drought. *Nature* **558**: 531–539.

Choat B, Jansen S, Brodribb TJ, Cochard H, Delzon S, Bhaskar R, Bucci SJ, Feild TS, Gleason SM, Hacke UG. 2012. Global convergence in the vulnerability of forests to drought. *Nature* **491**: 752–755.

Cowan IR, Farquhar GD. 1977. Stomatal function in relation to leaf metabolism and environment. *Symposium of the Society for Experimental Biology* **31**: 471–505.

Creek D, Lamarque LJ, Torres-Ruiz JM, Parise C, Burlett R, Tissue DT, Delzon S. 2020. Xylem embolism in leaves does not occur with open stomata: evidence from direct observations using the optical visualization technique. *Journal of Experimental Botany* **71**: 1151–1159.

Damour G, Simonneau T, Cochard H, Urban L. 2010. An overview of models of stomatal conductance at the leaf level. *Plant, Cell & Environment* **33**: 1419–1438.

Eller CB, Rowland L, Mencuccini M, Rosas T, Williams K, Harper A, Medlyn BE, Wagner Y, Klein T, Teodoro GS *et al.* 2020. Stomatal optimization based on xylem hydraulics (SOX) improves land surface model simulation of vegetation responses to climate. *New Phytologist* **226**: 1622–1637.

Eller CB, Rowland L, Oliveira RS, Bittencourt PR, Barros FV, Da Costa AC, Meir P, Friend AD, Mencuccini M, Sitch S. 2018. Modelling tropical forest responses to drought and El Niño with a stomatal optimization model based on xylem hydraulics. *Philosophical Transactions of the Royal Society of London. Series B: Biological Sciences* **373**: 20170315.

Farquhar GD, von Caemmerer S, Berry JA. 1980. A biochemical model of photosynthetic CO2 assimilation in leaves of C3 species. *Planta* **149**: 78–90.

Farquhar GD, Wong SC. 1984. An empirical model of stomatal conductance. *Australian Journal of Plant Physiology* **11**: 191–210.

Field C. 1983. Allocating leaf nitrogen for the maximization of carbon gain: leaf age as a control on the allocation program. *Oecologia* **56**: 341–347.

Fischer R, Rees D, Sayre K, Lu Z-M, Condon A, Saavedra AL. 1998. Wheat yield progress associated with higher stomatal conductance and photosynthetic rate, and cooler canopies. *Crop Science* **38**: 1467–1475.

Givnish TJ, Vermeij GJ. 1976. Sizes and shapes of liane leaves. *The American Naturalist* **110**: 743–778.

Guyot G, Scoffoni C, Sack L. 2012. Combined impacts of irradiance and dehydration on leaf hydraulic conductance: insights into vulnerability and stomatal control. *Plant, Cell & Environment* **35**: 857–871.

Haefner JW, Buckley TN, Mott KA. 1997. A spatially explicit model of patchy stomatal responses to humidity. *Plant, Cell & Environment* **20**: 1087–1097.

Hernandez-Santana V, Rodriguez-Dominguez CM, Fernández JE, Diaz-Espejo A. 2016. Role of leaf hydraulic conductance in the regulation of stomatal conductance in almond and olive in response to water stress. *Tree Physiology* **36**: 725–735.

Johnson D, McCulloh K, Meinzer F, Woodruff D, Eissenstat D. 2011. Hydraulic patterns and safety margins, from stem to stomata, in three eastern US tree species. *Tree Physiology* **31**: 659–668.

Jones HG, Sutherland RA. 1991. Stomatal control of xylem embolism. *Plant, Cell & Environment* **14**: 607–612.

Klein T. 2014. The variability of stomatal sensitivity to leaf water potential across tree species indicates a continuum between isohydric and anisohydric behaviours. *Functional Ecology* **28**: 1313–1320.

Lavergne A, Voelker S, Csank A, Graven H, de Boer HJ, Daux V, Robertson I, Dorado-Liñán I, Martínez-Sancho E, Battipaglia G. 2020. Historical changes in the stomatal limitation of photosynthesis: empirical support for an optimality principle. *New Phytologist* **225**: 2484–2497.

Lawson T, Blatt MR. 2014. Stomatal size, speed, and responsiveness impact on photosynthesis and water use efficiency. *Plant Physiology* **164**: 1556–1570.

Lawson T, Vialet-Chabrand S. 2018. Speedy stomata, photosynthesis and plant water use efficiency. *New Phytologist* **221**: 93–98.

Li X, Blackman CJ, Peters JM, Choat B, Rymer PD, Medlyn BE, Tissue DT. 2019. More than iso/anisohydry: hydroscapes integrate plant water use and drought tolerance traits in 10 eucalypt species from contrasting climates. *Functional Ecology* **33**: 1035–1049.

Lu Y, Duursma RA, Farrior CE, Medlyn BE, Feng X. 2020. Optimal stomatal drought response shaped by competition for water and hydraulic risk can explain plant trait covariation. *New Phytologist* **225**: 1206–1217.

Lu Y, Duursma RA, Medlyn BE. 2016. Optimal stomatal behaviour under stochastic rainfall. *Journal of Theoretical Biology* **394**: 160–171.

Mäkelä A, Berninger F, Hari P. 1996. Optimal control of gas exchange during drought: theoretical analysis. *Annals of Botany* **77**: 461–467.

Martin-StPaul N, Delzon S, Cochard H. 2017. Plant resistance to drought depends on timely stomatal closure. *Ecology Letters* **20**: 1437–1447.

Mayr S, Kartusch B, Kikuta S. 2014. Evidence for air-seeding: watching the formation of embolism in conifer xylem. *The Journal of Plant Hydraulics* **1**: e0004.

Medlyn BE, Duursma RA, Eamus D, Ellsworth DS, Prentice IC, Barton CVM, Crous KY, De Angelis P, Freeman M, Wingate L. 2011. Reconciling the optimal and empirical approaches to modelling stomatal conductance. *Global Change Biology* **17**: 2134–2144.

Meinzer FC, Johnson DM, Lachenbruch B, McCulloh KA, Woodruff DR. 2009. Xylem hydraulic safety margins in woody plants: coordination of stomatal control of xylem tension with hydraulic capacitance. *Functional Ecology* **23**: 922–930.

Meinzer FC, Smith DD, Woodruff DR, Marias DE, McCulloh KA, Howard AR, Magedman AL. 2017. Stomatal kinetics and photosynthetic gas exchange along a continuum of isohydric to anisohydric regulation of plant water status. *Plant, Cell & Environment* **40**: 1618–1628.

Papanatsiou M, Petersen J, Henderson L, Wang Y, Christie J, Blatt M. 2019. Optogenetic manipulation of stomatal kinetics improves carbon assimilation, water use, and growth. *Science* **363**: 1456–1459.

Pearcy RW. 1990. Sunflecks and photosynthesis in plant canopies. *Annual Review of Plant Physiology* **41**: 421–453.

Pivovaroff AL, Cook VM, Santiago LS. 2018. Stomatal behaviour and stem xylem traits are coordinated for woody plant species under exceptional drought conditions. *Plant, Cell & Environment* **41**: 2617–2626.

Prentice IC, Dong N, Gleason SM, Maire V, Wright IJ. 2014. Balancing the costs of carbon gain and water transport: testing a new theoretical framework for plant functional ecology. *Ecology Letters* **17**: 82–91.

Reichstein M, Tenhunen JD, Roupsard O, Ourcival J, Rambal S, Miglietta F, Peressotti A, Pecchiari M, Tirone G, Valentini R. 2002. Severe drought effects on ecosystem CO2 and H2O fluxes at three Mediterranean evergreen sites: revision of current hypotheses? *Global Change Biology* **8**: 999–1017.

Sack L, John GP, Buckley TN. 2018. ABA accumulation in dehydrating leaves is associated with decline in cell volume, not turgor pressure. *Plant Physiology* **176**: 489–495.

Salter WT, Merchant AM, Richards RA, Trethowan R, Buckley TN. 2019. Rate of photosynthetic induction in fluctuating light varies widely among genotypes of wheat. *Journal of Experimental Botany* **70**: 2787–2796.

Salvi AM, Smith DD, Adams MA, McCulloh KA, Givnish TJ. 2021. Mesophyll photosynthetic sensitivity to leaf water potential in Eucalyptus: a new dimension of plant adaptation to native moisture supply. *New Phytologist* **230**: 1844–1855.

Sharpe PJH, Wu H, Spence RD. 1987. Stomatal mechanics. In: Zeiger E, Farquhar GD, Cowan IR, eds. *Stomatal function*. Stanford, CA, USA: Stanford University Press, 91–114.

Sperry JS. 2004. Coordinating stomatal and xylem functioning – an evolutionary perspective. *New Phytologist* **162**: 568–570.

Sperry JS, Venturas MD, Anderegg WR, Mencuccini M, Mackay DS, Wang Y, Love DM. 2017. Predicting stomatal responses to the environment from the optimization of photosynthetic gain and hydraulic cost. *Plant, Cell & Environment* **40**: 816–830.

Sperry JS, Wang Y, Wolfe BT, Mackay DS, Anderegg WR, McDowell NG, Pockman WT. 2016. Pragmatic hydraulic theory predicts stomatal responses to climatic water deficits. *New Phytologist* **212**: 577–589.

Taylor SH, Long SP. 2017. Slow induction of photosynthesis on shade to sun transitions in wheat may cost at least 21% of productivity. *Philosophical Transactions of the Royal Society of London. Series B: Biological Sciences* **372**: 20160543.

Vico G, Manzoni S, Palmroth S, Katul G. 2011. Effects of stomatal delays on the economics of leaf gas exchange under intermittent light regimes. *New Phytologist* **192**: 640–652.

Wang Y, Sperry JS, Anderegg WR, Venturas MD, Trugman AT. 2020. A theoretical and empirical assessment of stomatal optimization modeling. *New Phytologist* **227**: 311–325.

de Wit C. 1965. *Photosynthesis of leaf canopies. Agriculture research report.* Wageningen, the Netherlands: Centre for Agricultural Publication and Documentation (PUDOC).

Wolf A, Anderegg WR, Pacala SW. 2016. Optimal stomatal behavior with competition for water and risk of hydraulic impairment. *Proceedings of the National Academy of Sciences, USA* **113**: E7222–E7230.

Zwieniecki MA, Holbrook NM. 2009. Confronting Maxwell's demon: biophysics of xylem embolism repair. *Trends in Plant Science* **14**: 530–534.

Appendix A1 Additional details of model

Dynamical model

We modeled stomatal conductance to water vapor (g_{sw}) as a linear combination of guard cell and epidermal turgor pressures (P_g and P_e, respectively):

$$g_{sw} = \chi\left(P_g - mP_e\right) = \chi(\delta\pi - M(\psi_{leaf} + \pi_e)) \qquad \text{Eqn A1}$$

where m is the epidermal mechanical advantage, χ is a scaling factor (which we assumed to be constant), $\delta\pi$ is the guard cell osmotic gradient (the difference in osmotic pressure between guard and epidermal cells), $M \equiv m - 1$ is the net epidermal mechanical advantage, and π_e is epidermal osmotic pressure. Eqn A1 assumes that guard cell and epidermal water potentials are equal to each other and to the bulk-leaf value green, ψ_{leaf}, calculated from stem and leaf hydraulic conductances, soil water potential, and transpiration rate, as described later. We also assumed that π_e was equal to bulk-leaf osmotic pressure, and thus changed passively in

relation to leaf water content as described in Eqn A4 below, and that g_{sw} could not reach precisely zero, but was instead limited to be greater than or equal to a value g_{min} (nominally 0.005 mol m^{-2} s^{-1}).

We predicted the 'target' value of stomatal conductance at any given time (g'_{sw}) using Eqns 1 and 2 (with net CO_2 assimilation rate, A, calculated using a biochemical model; Supporting Information Methods S1), solved numerically using the *optimize*() function in JULIA with a Golden Section search algorithm bounded between $g_{sw} = 0$ and 2.0 mol m^{-2} s^{-1}. We assumed that the guard cell osmotic gradient, $\delta\pi$, changes at a rate proportional to the difference between its current value and a target value $\delta\pi'$, with a rate constant α_π (which differed when $\delta\pi$ was increasing or decreasing):

$$\frac{d\delta\pi}{dt} = \alpha_\pi(\delta\pi' - \delta\pi) \qquad \text{Eqn A2}$$

where $\delta\pi'$ is the value of $\delta\pi$ needed to make g_{sw} equal to g'_{sw}, and is related to g'_{sw} as

$$g'_{sw} = \chi(\delta\pi' - M(\psi_{leaf} + \pi_e)). \qquad \text{Eqn A3}$$

Thus, $\delta\pi' - \delta\pi = (g'_{sw} - g_{sw})/\chi$. This latter relation may seem to suggest that g_{sw} could be modeled more directly, without reference to $\delta\pi$, using an equation analogous to Eqn A2; however, that would not account for the interactive roles of leaf water potential and $\delta\pi$ in generating dynamic features of stomatal responses that may be important in hydraulic risk (e.g. the transient 'wrong-way' responses of stomata to changes in water status; Buckley *et al.*, 2011).

We modeled leaf water potential as a function of leaf relative water content, R, following Sack *et al.* (2018):

$$\psi_{leaf} = \pi_o \cdot \max\left\{\frac{R - R_{tlp}}{1 - R_{tlp}}, 0\right\} - \frac{\pi_o}{R} \qquad \text{Eqn A4}$$

where π_o is leaf osmotic pressure (>0) at full turgor and R_{tlp} is leaf relative water content at the turgor loss point; the term involving max{} represents cell turgor, which we assume cannot be negative; the term π_o/R is osmotic pressure. To model R dynamically, we expressed it in terms of the number of moles of water in the leaf, n_{leaf}:

$$R = \frac{n_{leaf}}{n_{leaf,max}} \qquad \text{Eqn A5}$$

where $n_{leaf,max}$ is the value of n_{leaf} at full turgor. The rate of change of n_{leaf} equals the difference between the rate of water flow into the leaf from the stem and the transpiration rate:

$$\frac{dn_{leaf}}{dt} = K_{leaf}(\psi_{stem} - \psi_{leaf}) - E \qquad \text{Eqn A6}$$

where K_{leaf} is leaf hydraulic conductance, ψ_{stem} is stem water potential, and E is leaf transpiration rate, given by

$$E = \frac{g_{sw} g_{bw}}{g_{sw} + g_{bw}} \Delta w, \qquad \text{Eqn A7}$$

where Δw is the leaf-to-air water vapor mole fraction gradient and g_{bw} is leaf boundary layer conductance to water vapor. We calculated Δw from leaf temperature (T_{leaf}, simulated dynamically; Eqn A12) and ambient water vapor mole fraction (w_{air}) as $\Delta w = w_{sat}(T_{leaf}) - w_{air}$, where $w_{sat}(T_{leaf})$ is the saturation water vapor mole fraction. ψ_{stem} depends on stem water content, n_{stem}. We assumed a linear relationship between ψ_{stem} and n_{stem} and hence a fixed elastance (sensitivity of water potential to relative water content), e_{stem}: $\psi_{stem} = e_{stem} \cdot (n_{stem}/n_{stem,max} - 1)$, where $n_{stem,max}$ is the value of n_{stem} at a water potential of zero. Stem water content changes as the balance of water flow in from the soil and out to the leaf:

$$\frac{dn_{stem}}{dt} = K_{stem}(\psi_{soil} - \psi_{stem}) - K_{leaf}(\psi_{stem} - \psi_{leaf}) \qquad \text{Eqn A8}$$

where K_{stem} is stem hydraulic conductance and ψ_{soil} is soil water potential. Although this formulation does not explicitly incorporate root hydraulics, K_{stem} and n_{stem} can be interpreted as including the contributions of roots to water transport and storage.

We assumed that leaf and stem hydraulic conductances both declined with water potential according to a hydraulic vulnerability curve:

$$K'_{j25} = \frac{K'_{j25max}}{1 + \left(\frac{\psi_j}{\psi_{j50}}\right)^{\xi}} \qquad \text{Eqn A9}$$

where the subscript j refers to either leaf or stem, ψ_{j50} is the water potential at which conductivity is reduced by half, and ξ is a dimensionless empirical parameter. Eqn A9 refers to values of K at 25°C because only the anatomical (temperature-independent) component of hydraulic conductance is reduced by embolism formation. Independent of embolism formation, we also allowed K_j to vary with temperature as $K_j(T) = K_{j25} \cdot (T_{leafK}/298.15)^7$ (where T_{leafK} is in kelvins) due to the temperature dependence of viscosity.

Embolisms take a finite period of time to expand to fill a conduit; 'primes' in Eqn A9 refer to equilibrium values after embolism expansion was completed, and each hydraulic conductance was simulated dynamically using Eqn A10:

$$\frac{dK_{j25}}{dt} = \alpha_K\left(K'_{j25} - K_{j25}\right) \qquad \text{Eqn A10}$$

where α_K is an empirical rate constant. The true rate of embolism expansion is unknown. Some evidence suggests that air-seeded embolisms expand to fill conduits within milliseconds (Mayr *et al.*, 2014). However, using an appropriately fast rate constant in Eqn A10 makes the overall system of differential equations intractably stiff (i.e. having rates of change that differ by many orders of magnitude among variables). One solution would be to treat hydraulic conductances as quasi-static with respect to

variations in water potential; that is, simply use Eqn A9 rather than modeling them dynamically. However, that solution is not suitable in this context, because embolism-induced declines in K are generally irreversible in the short term: embolism repair must wait for water potential to recover to near zero overnight (Brodersen & McElrone, 2013). Treating K as quasi-static with respect to water potential would require treating Eqn A9 as a time-independent state function, which is irreconcilable with the irreversible nature of declines in K. To capture irreversible changes, it is necessary to account explicitly for the direction of change in K at any moment. We resolved this dilemma by setting dK_{j25}/dt to zero whenever water potential, and hence K_{j25}, is increasing (i.e. $K'_{j25} > K_{j25}$), but when water potential and K_{j25} are decreasing, using Eqn A10 with a very small value of the rate constant α_K (namely, the smallest value that led to stable solutions, $\alpha_K = 0.2$; i.e. step declines in hydraulic conductance were 63.2% complete in 5 s):

$$\frac{dK_{j25}}{dt} = \begin{cases} \alpha_K\left(K'_{j25} - K_{j25}\right) & \text{if } K'_{j25} < K_{j25} \\ 0 & \text{else} \end{cases} \quad \text{Eqn A11}$$

Evaporative demand (Δw) and K_{leaf}, as well as key parameters of photosynthesis, depend on leaf temperature, T_{leaf}. The rate of change of T_{leaf} equals the difference between the rate of energy inputs to the leaf and the rate of energy losses, all divided by the leaf heat capacitance, k_{leaf}:

$$\frac{dT_{leaf}}{dt} = \frac{Q_{SW} + f_{ir}\epsilon_{sky}\sigma T_{airK}^4 - f_{ir}\epsilon\sigma T_{leafK}^4 - c_{pa}g_{bh}(T_{leaf} - T_{air}) - \lambda E}{\kappa_{leaf}} \quad \text{Eqn A12}$$

where Q_{SW} is the absorbed shortwave radiation flux, ε_{sky} is sky emissivity, ε is leaf emissivity, σ is the Stefan–Boltzmann constant, c_{pa} is the heat capacity of the air, g_{bh} is the boundary layer conductance to heat (a whole-leaf, two-sided value), T_{air} is air temperature (T_{airK} in kelvins), λ is the latent heat of vaporization, and κ_{leaf} is leaf heat capacity (J m^{-2} K^{-1}). f_{ir} is the longwave sky-view factor of the target leaf (the rate of thermal infrared exchange between the leaf and the atmosphere as a fraction of the rate that would occur for an otherwise identical leaf at the top of the canopy, unobstructed by other canopy elements). Eqn A12 ignores net IR exchange at the lower leaf surface, in effect assuming the average temperature of lower canopy elements is equal to that of the target leaf. We estimated Q_{SW} and f_{ir} for each leaf using the Helios model (see Methods S5). We calculated ε_{sky} as $0.642(w_{air}\cdot 10^5/T_{airK})^{1/7}$ (Brutsaert, 1975), where 10^5 (Pa) is atmospheric pressure, which converts w_{air} to a partial pressure. We calculated K_{leaf} from leaf water content (n_{leaf}, mol m^{-2}) and leaf dry mass per unit area (LMA, nominally 140 g m^{-2}) as: $K_{leaf} = 4.184\cdot 18.01\cdot n_{leaf} + 1.5\cdot$LMA, where 4.184 (J g^{-1}) is the heat capacity of water, 18.01 (g mol^{-1}), and 1.5 (J g^{-1}) is the heat capacity of leaf dry matter. We assumed T_{air} varied sinusoidally over time during the daylight hours, thus: $T_{air} = T_{airmin} + (T_{airmax} - T_{airmin})\cdot\sin(0.5\pi(\text{time} - 5)/(t_{Tairmax} - 5))$, where time is time of day in hours, $t_{Tairmax}$ = 13 h, T_{airmin} = 15°C and T_{airmax} = 25°C.

We simulated the maximum velocity of RuBP carboxylation at 25°C (V_{m25}) dynamically, to capture finite kinetics of photosynthetic induction under fluctuating PPFD:

$$\frac{dV_{m25}}{dt} = \alpha_V\left(V'_{m25} - V_{m25}\right) \quad \text{Eqn A13}$$

where α_v is an empirical rate constant and V'_{m25} is the target value of V_{m25}, calculated as a saturating function of PPFD: V'_{m25} = (fully induced V_{m25})·PPFD/(PPFD + K_{mv}). Thus, V'_{m25} is half of the fully induced value when PPFD = K_{mv} (nominally 97 μmol m^{-2} s^{-1}). We assumed the fully induced V_{m25} varied across leaves in proportion to daily mean PPFD (such that (fully induced V_{m25}) = 0.25·(mean PPFD), where V_{m25} and PPFD have units of μmol m^{-2} s^{-1}). We also assumed the values of K_{leaf} and K_{stem} at 25°C and water potentials of zero ($K_{leaf25max}$ and $K_{stem25max}$, respectively) were equal to one another but varied among leaves in proportion to fully induced photosynthetic capacity, such that $K_{leaf25max} = K_{stem25max}$ = 0.01·(fully induced V_{m25}) = 0.025·(mean PPFD), where $K_{leaf25max}$ and $K_{stem25max}$ have units of mol m^{-2} s^{-1} MPa^{-1}.

We computed net CO_2 assimilation rate from g_{sw}, T_{leaf}, V_{m25}, and PPFD using the Farquhar *et al.* (1980) biochemical model (Methods S1), assuming that values of potential electron transport rate and nonphotorespiratory CO_2 release in the light were proportional to V_{m25}.

Simulation of PPFD dynamics

The main environmental driver of short-term dynamics in the model is PPFD; we assumed ambient H_2O and CO_2 concentrations are constant and air temperature varies sinusoidally over the day. We used the Helios reverse ray-tracing-based model (v.1.2.8; Bailey, 2018, 2019) to simulate diurnal trends of absorbed PPFD (direct + diffuse) and ambient longwave radiation in realistic canopies. The simulated canopy had a leaf area index of 2.5 and was 1 m tall with a horizontal extent of 5 m × 5 m, although a periodic boundary condition was applied to effectively simulate a horizontally infinite canopy. The 3D spatial position and angle (normal vector) of each leaf were selected randomly from specified inclination distributions. Most simulations assumed a spherical inclination distribution and vertically and horizontally homogeneous spatial distributions of leaves; additional simulations varied inclination distributions (spherical, planophile, and erectophile, *sensu* de Wit, 1965) and used spatially clumped distributions of leaves representing trees with homogeneous spherical crowns (i.e. no sub-crown clumping) and an LAI of 2.5 (calculated on the basis of total ground area, i.e. including not only the projected area of each individual crown, but also the ground area in between individual crowns). We randomly selected 10 000 1 cm × 1 cm leaf patches from the total of 625 000 patches (25 000 leaves × 25 patches per leaf). For

each leaf patch, we converted the temporally discrete (0.1 Hz) series of PPFD values generated by Helios into a continuous function of PPFD vs time using cubic spline interpolation (*Spline1D*() function in the DIERCKX package in JULIA v.1.5.3; see Methods S5 for more details).

Numerical methods

PPFD time series from Helios for each patch were output to file. Physiological simulations were performed in JULIA v.1.5.3. We solved the system of coupled differential equations describing time evolution of physiological variables numerically, using the functions *ODEProblem*() and *solve*() from JULIA package *DifferentialEquations.jl*. We allowed *solve*() to choose the optimal algorithm (usually a composite of the *Tsit5*() and *Rosenbrock23*() algorithms; respectively, a fourth-order Runge Kutta algorithm, and an order 2/3 L-stable Rosenbrock-W method suitable for stiff systems). We interpolated solution values at 0.1 Hz using the package's default interpolation algorithms. Initial conditions (values at the beginning of the day, which are needed to initialize the numerical solutions) were set as follows: leaf and stem water contents were saturated, leaf and stem hydraulic conductances were equal to their maximum values, leaf temperature equaled air temperature, the activation state of photosynthetic capacity was set to 100%, and guard cell osmotic pressure was set to give a stomatal conductance of zero at a water potential of zero. Simulation code is included as Methods S6 and will be made available in a public GitHub repository upon publication. Code for Helios is available in a public GitHub repository at (https://www.github.com/PlantSimulationLab/Helios).

Supporting Information

Additional Supporting Information may be found online in the Supporting Information section at the end of the article.

Fig. S1 Illustration of wavelet analysis of sunflecks.

Fig. S2 Distributions of sunfleck strength vs canopy structure.

Fig. S3 Measures of sunfleck strength vs minimum leaf water potential.

Fig. S4 Effect of photosynthetic induction rate on economics of short-term risk.

Fig. S5 Physiological kinetics for square-wave sunfleck.

Fig. S6 Optimal ψ_{50risk} vs canopy structure.

Fig. S7 Sample physiological dynamics during a single sunfleck.

Fig. S8 Effect of ψ_{50risk} on total carbon gain and final PLC during a sunfleck.

Fig. S9 Sensitivity of mean daily photosynthesis to variation in plant-related parameters.

Fig. S10 Sensitivity of mean daily minimum leaf water potential to variation in plant-related parameters.

Fig. S11 Sensitivity coefficients from sensitivity analysis.

Fig. S12 Sensitivity of photosynthesis and water potential to variation in environmental parameters.

Fig. S13 Effect of variation in epidermal mechanical advantage.

Fig. S14 Best-fit and hydraulics-based penalty functions from Eller *et al.* (2020).

Methods S1 Photosynthesis model.

Methods S2 Quantifying sunfleck properties by wavelet analysis.

Methods S3 Parameter estimation.

Methods S4 Parameter sensitivity analysis.

Methods S5 Canopy radiation penetration modeling with Helios.

Methods S6 JULIA code and dependencies.

Please note: Wiley is not responsible for the content or functionality of any Supporting Information supplied by the authors. Any queries (other than missing material) should be directed to the *New Phytologist* Central Office.